Earth's Future

RESEARCH ARTICLE
10.1029/2023EF003924

A National-Scale Coastal Flood Hazard Assessment for the Atoll Nation of Tuvalu

Moritz Wandres[1,2], Antonio Espejo[1,2], Tomasi Sovea[1,2], Sapolu Tetoa[3], Faatasi Malologa[3], Arthur Webb[4], James Lewis[5], Gary Lee[1,2], and Hervé Damlamian[1,2]

[1]Geoscience, Energy and Maritime (GEM) Division, Pacific Community (SPC), Suva, Fiji, [2]Pacific Community Centre for Ocean Science (PCCOS), Pacific Community, Suva, Fiji, [3]Lands and Survey Department, Government of Tuvalu, Funafuti, Tuvalu, [4]Resilience & Sustainable Development Unit, United Nations Development Programme (UNDP), Suva, Fiji, [5]Intercoastal Consulting, Burleigh Heads, QLD, Australia

Abstract Atoll nations such as Tuvalu are considered to be amongst those most vulnerable to the effects of climate change. Here we present a national-scale coastal flood hazard assessment for Tuvalu based on high-resolution Light Detection and Ranging (LiDAR) topography and bathymetry. We follow a fully probabilistic approach, considering sea level anomalies, tides, and extreme wave conditions from a mixed climate (i.e., from distant extra-tropical storms and local tropical cyclones). Nearshore processes such as wave setup and runup are also accounted for. Hazard maps were calculated for the present sea level, as well as for sea level rise projections corresponding to different shared socioeconomic pathways (SSP2 4.5 and SSP5 8.5) and time horizons (2060 and 2100). With a mean elevation of 1.55 m above mean sea level (1.37 m above mean high water spring) >25% of land area is inundated once every 5 years and >50% of land area floods once every 100 years nationally. Results indicate that present day 1-in-50 years floods (>45% of land area flooded) will occur more than once every 5 years by 2060 (annual exceedance probability >20%), even under the moderate SSP2 4.5 sea level rise projections. Results of this study highlight the pressing need for ambitious and large-scale adaptation solutions which are commensurate with projected sea level rise and marine hazard impacts. The methodologies presented in this paper can easily be applied to other low-lying islands in the tropical Pacific, where mixed climates (i.e., regular and TC conditions) and non-linear nearshore processes dominate extreme water levels and flooding.

Plain Language Summary Low-lying atoll nations such as Tuvalu are widely recognized to be amongst those most impacted by the effects of climate change. To make informed adaptation decisions, accurate baseline data (i.e., topography and bathymetry) and marine hazard information are fundamental. In this paper we present a national-scale coastal flood hazard assessment for Tuvalu based on state-of-the art high-resolution baseline data and statistical and numerical models. We considered the present-day sea levels and sea level rise projections corresponding to different climate change scenarios. Under present-day sea levels >25% of Tuvalu's land area floods once every 5 years and >50% of land area floods once every 100 years. Our results indicate a significant increase in severity and frequency of extreme coastal flooding due to climate change with present-day 1-in-50-year floods occurring more than once every 5 years by 2060. This study highlights the pressing need for ambitious and large-scale adaptation solutions. The methodology presented here is suitable to be used in other Pacific Island locations.

Key Points:

- We present a probabilistic flood hazard assessment of Tuvalu considering tides, sea level anomalies, storm surges, and waves from a mixed climate (i.e., generated by tropical and extratropical storms)
- A mean elevation of 1.55 m above MSL makes Tuvalu highly vulnerable to wave driven flooding with >25% of land area inundated once every 5 years
- Present day 1-in-50 years floods (>45% of land area flooded) will occur more than once every 5 years by 2060 due to sea level rise

Supporting Information:

Supporting Information may be found in the online version of this article.

Correspondence to:

M. Wandres,
moritzw@spc.int

Citation:

Wandres, M., Espejo, A., Sovea, T., Tetoa, S., Malologa, F., Webb, A., et al. (2024). A national-scale coastal flood hazard assessment for the atoll nation of Tuvalu. *Earth's Future*, *12*, e2023EF003924. https://doi.org/10.1029/2023EF003924

Received 26 JUN 2023
Accepted 1 MAR 2024

1. Introduction

Small Island States are widely recognized to be amongst those most impacted by the effects of climate change (Mycoo et al., 2022). Recent studies project a significant increase in the frequency and extent of coastal flooding in the tropical Pacific (Shope et al., 2016; Vitousek et al., 2017), posing a strong risk to the habitability of many atolls and low-lying reef islands over the coming decades (Storlazzi et al., 2018). This is particularly the case when considering other risk factors such as freshwater or land-based food supply (Duvat et al., 2021). A detailed localized understanding of the coastal inundation hazard of atolls is therefore critical for targeted adaptation and resource prioritization. The island nation of Tuvalu is one of the few countries in the world that consists exclusively of low-lying atolls and reef islands. As such, the country and Tuvaluan People are particularly vulnerable to coastal flooding (Duvat et al., 2021; Taupo et al., 2018). For example, in 2015 most of Tuvalu's islands were severely impacted by large waves, generated by distant-source tropical cyclone (TC) Pam (Hoeke et al., 2021). In 2018, a large swell generated by an extra-tropical low-pressure system in the Southern Ocean and

Tasman Sea caused extensive flooding in some of Tuvalu's southern islands (Tuvalu Meteorological Service, 2018). Additionally, to large waves generated by distant storms, Tuvalu also experiences direct hits from TCs (such as TC Bebe in 1972) and associated extreme wave and water level conditions (e.g., Maragos et al., 1973). Apart from relatively frequent wave-driven inundation events, many low-lying areas in Tuvalu regularly flood during spring tides as marine water percolates through the porous limestone and temporarily fills depressions at the surface (Patel, 2006; Yamano et al., 2007).

Coastal inundation in fringing-reef environments often occurs as a compound event, where waves, tides, and sea level anomalies all interact non-linearly to generate extreme total water levels (TWLs) and flooding (e.g., Becker et al., 2014; Ford et al., 2018; Hoeke et al., 2013; Wandres et al., 2020).

There are two important wave-driven mechanisms that contribute to nearshore water levels on reef-mediated shores such as the islands of Tuvalu (e.g., Beetham et al., 2016). Waves dissipate as they break on the reef edge and the excess momentum flux in the water column causes a steady elevation of the mean still water surface (e.g., Becker et al., 2014). On reef-fronted islands, this effect (called wave setup) has been found to reach up to one third of the incident offshore wave heights (Munk & Sargent, 1948; Tait, 1972; Vetter et al., 2010). The dissipation of swell groups also generates infragravity (IG) waves (bore-like uprush of individual waves onto the beach), which can significantly contribute to the total runup, which can be defined as the sum of wave setup, IG waves, and waves in the sea and swell frequency bands (Baldock, 2012; Beetham et al., 2016; Pomeroy et al., 2012; van Dongeren et al., 2013). Wave setup and IG waves are strongly modulated by the offshore water level conditions (i.e., tides and sea level anomalies; Beetham et al., 2016).

The multivariate nature of wave-driven flooding makes the determination of wave driven inundation intensity and likelihood challenging. Hoeke et al. (2021) recently investigated nearshore extreme TWLs in Tuvalu over a 40-year period using an empirical equation by Merrifield et al. (2014). The methodology allowed to assign a probability to historical flood events such as the severe inundation from distant tropical cyclone (TC) Pam in 2015. While this is useful in terms of risk knowledge and community awareness, the methodology does not (and was not intended to) provide actionable hazard information such as flood depth and extent. Process-based numerical models such as XBeach (Roelvink et al., 2009) or SWASH (Zijlema et al., 2011) have been shown to accurately resolve the nonlinear processes associated with reef-fronted flooding (e.g., Buckley et al., 2014; Quataert et al., 2015; Storlazzi et al., 2018). However, these models are computationally expensive, making their usage over large areas difficult and time consuming. To address this, Pearson et al. (2017) developed a Bayesian-based system to assess wave-driven flooding on reef-fronted coasts by creating a large synthetic database of XBeach simulations. Rueda et al. (2019) expanded on the work by applying an interpolation technique to efficiently obtain runup estimations for infinite combinations of reef-morphologies and oceanographic forcings. More recently, Liu et al. (2023) developed an explicit wave-runup formula based on Pearson et al.'s (2017) database. However, the synthetic database of simulations only includes waves smaller than 5 m, making it unsuitable for areas with TCs (i.e., where wave heights are exceeding 5 m).

Other studies investigating exceedance probabilities of extreme TWLs in areas of TCs indicated some issues in estimating return intervals for rare extreme TWLs using conventional methods such as Generalized Extreme Value (GEV) distribution. First, the infrequency of TCs often fails to capture TC-driven extreme TWLs of longer return periods, particularly when basing the extreme value analysis on short observation periods (e.g., Haigh et al., 2014; O'Grady et al., 2019). Second, in areas where TCs and distant-storms (along with tides and atmospheric variability) modulate TWLs, the mixed nature of the extreme value distributions requires special consideration (O'Grady et al., 2022).

Here we present a novel, comprehensive approach to assess probabilistic inundation hazard in reef-fronted islands, accounting for all relevant drivers of coastal inundation, that is, waves generated by tropical cyclones, extra-tropical storms, tides, and sea level anomalies. Nearshore processes such as wave setup and runup (e.g., IG wave motions) are also accounted for. The hazard assessment is based on state-of-the-art Light Detection and Ranging (LiDAR) bathymetry and topography data.

Tuvalu's National Strategy for Sustainable Development 2021–2030 ("Te Kete") sets out the nation's high-level strategic plan to achieve "a peaceful, resilient and prosperous Tuvalu" (Government of Tuvalu, 2020). National outcome 4 of Te Kete is focused on increased climate change and disaster resilience. The coastal hazard information presented in this paper are fundamental for Tuvalu to make science-informed adaptation decisions.

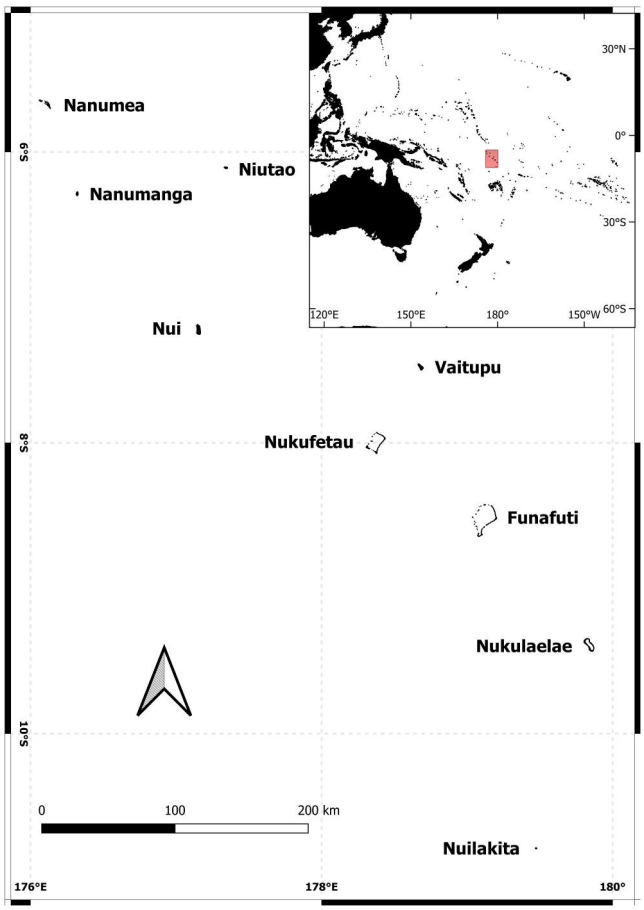

Figure 1. Map of Tuvalu and its nine atolls.

The paper is structured as follows: Section 2 describes the study site and the oceanographic conditions of Tuvalu. The underlying data are described in Section 3. The methodology to derive extreme offshore ocean conditions is outlined in Section 4 and the inundation modeling approach is described in Section 5. Results are presented in Section 6 and discussed in Section 7.

2. Study Site

Tuvalu consists of nine atolls and low-lying reef islands (Figure 1). The country has a population of 10,645 people according to a 2017 census (Government of Tuvalu, 2017), with the majority living in the capital atoll of Funafuti and with the entire population living a few meters from the coastline (Andrew et al., 2019). Like other coral reef islands, Tuvalu's islands consist of unconsolidated and/or poorly lithified carbonate sand and gravel deposits on top of coral reef platforms (Webb & Kench, 2010). Five of the islands are classified as true atolls (Nanumea, Nui, Nukufetau, Funafuti, and Nukulaelae), meaning they have an essentially continuous rim of reef at or near the surface of the sea which surrounds a deeper lagoon. Three of the islands are classified as table reefs (Nanumaga, Niutao, and Niulakita), meaning they have a continuous land margin that completely encircles a shallow enclosed lagoon(s) or pond(s). Vaitupu possesses both characteristics of a table reef and atoll thus does not strictly conform to either definition, in that its two small lagoons are almost completely enclosed by land (Mclean & Hosking, 1991). Tuvalu's islands are all low-lying and while various values for land area and mean elevation can be found in the literature and online, no high-resolution country-scale topographic survey had been performed prior to this study.

Few studies have investigated Tuvalu's wave climate (e.g., Barstow & Haug, 1994; Bosserelle et al., 2015b; Durrant et al., 2014), however, these studies were based on either relatively coarse global wave hindcasts or short term in situ observations. More recently, Wandres et al. (2023) developed a 44-year (1979–2022) high-resolution wave hindcast of Tuvalu. The authors identified three main wave sources: mid-latitude storms in the Southern Ocean and in the North Pacific, easterly trade winds, and tropical cyclones. It was found that Tuvalu's wave climate is closely linked to large-scale climate modes such as the El Niño Southern Oscillation (ENSO), Pacific Decadal Oscillation (PDO), and Arctic and Antarctic Oscillation (AO and AAO).

Funafuti has a maximum tidal range of 2.4 m (Ritman et al., 2022). Sea level rise trends in Tuvalu based on tide gauge records between 1993 and 2008 were estimated to be 5.9 mm/year with negligible impact from vertical land movement (Aung et al., 2009). More recently, the Guidance for Managing Sea Level Rise Infrastructure Risk in Pacific Island Countries report analyzed rates of sea level rise from tide gauges across the Pacific and found a rate of 4.84 mm/year in Tuvalu (PRIF, 2021). Other recent studies investigating SLR in the South Pacific over longer time periods found similar trends. For example, a recent study deriving sea level trends from satellite altimetry estimated an increase in sea level in Tuvalu of 13 ± 7 cm (~4.82 mm/year) between 1993 and 2020 (Marra et al., 2022).

3. Data

3.1. Bathymetry and Topography

Most islands in the Pacific region have no established vertical reference datum and in turn no locally referenced mean sea level. Without mapping the topography and referencing it to the sea level, accurately assessing coastal hazards and the long-term impacts of sea level rise on low-lying communities is impossible.

Light Detection and Ranging (LiDAR) is a remote sensing method that uses light in the form of a pulsed laser to measure variable distances to the Earth. LiDAR surveys provide accurate (horizontal and vertical errors <10 cm) and high-resolution point cloud data that can be interpolated onto digital elevation models (DEMs). Due to their

Table 1
Maximum Elevation of Tuvalu's Islands Derived From the LiDAR DEM

Island name	Max. elevation (m)	Point description
Funafuti	6.93	The highest point is located near Queen Elisabeth Park which is a pile of sand that was used for leveling the surface of the reclaimed land on the main islet before Pacific Island Forum meeting 2019
Nanumea	6.71	The highest point is located on Lakena islet, a pulaka pit (swamp taro) farming area for locals, thus the point is likely man-made
Nanumaga	10.48	The three highest points are all situated near pulaka pits. They are related to spoil mounds from pulaka pit excavations
Nukulaelae	10.48	The highest point is located on Fagaua islet near a pulaka pit. Thus, it is most likely a result of human activity
Vaitupu	7.68	The two highest points to the north side of the island are situated in the densest area of pulaka pits. They both are likely man-made. Another similarly high point to the south of the island is part of the village, thus it could be a natural or man-made point
Nukufetau	5.81	The highest point in Nukufetau is on Fale Islet. The islet is the farming area for locals with pulaka pits and a piggery farm. Thus, the highest point of the island is man-made
Niulakita	6.54	The highest point in Niulakita seems to be the natural storm berm with no apparent structures or pulaka pits nearby
Nui	8.37	The highest points on Fenuatapu (Mainland) and Meang islet are the results of human intervention. Both are located near pulaka pits
Niutao	8.67	The highest point in Niutao is a result of human intervention (pulaka pit)

Note. Description of the points were obtained from the Government of Tuvalu Lands and Survey Department.

high cost, LiDAR surveys generally only focus on densely populated or otherwise high-priority areas. Through the Tuvalu Coastal Adaptation Project (TCAP), the United Nations Development Programme (UNDP) contracted Fugro to collect nationwide airborne LiDAR topography and bathymetry data (FUGRO, 2019).

The initial data collection was reduced to the Geodetic Reference System 1980 (GRS80) ellipsoid. Strategic benchmarks on all nine atolls were occupied and linked to temporary tide gauges by the Tuvalu Lands and Survey Department and the Pacific Community (SPC) to reduce the final data to a local reference datum (MSL).

LiDAR data were seamlessly blended with multi-beam bathymetry data previously collected by SPC (formerly SOPAC; Krüger, 2008). The multi-beam data covered water depths of ∼10 m up to ∼2,000 m around all of Tuvalu's nine atolls. Beyond the areas of in situ bathymetric data, the General Bathymetric Chart of the Oceans (GEBCO) was used.

Tables 1 and 2 display the maximum and mean elevation above MSL for all islands and the entire country obtained from the LiDAR DEM. Mean elevations were calculated using two different methods: (a) the average elevation of the areas above mean sea level (MSL); (b) the average elevation of all areas above mean high water spring tide (MHWS). These two methods were used as some sandbanks and reefs might be exposed at mid-tide. The 2nd method therefore gives a better estimate of Tuvalu's inhabitable land area.

The highest points in Tuvalu are in Nanumaga and Nukulaelae (both ∼10.5 m above MSL; Table 1). However, these points are results of anthropogenic activities through dredging of pulaka (swamp taro) pits. On most other atolls, the highest points were also the results of human intervention. The highest natural points in Tuvalu are in Niulakita and Nanumaga (both approximately 6.5 m above MSL) and in both cases these elevations are associated with the ocean-side storm berm landforms of the islands. Across all nine islands, the most elevated naturally occurring land is consistently associated with these oceanside nearshore storm berm features, which accreted due to the deposition of carbonate sediment during inundation events (Mclean & Hosking, 1991).

Overall, Tuvalu has a land area of 38.69 km^2 above MSL and a mean elevation of 1.55 m above MSL (Table 2). Keeping in mind the tidal range is approximately 2 m this means large areas of Tuvalu are exposed to high tides. A better estimate of the habitable area is therefore to use MHWS as a reference datum. Across all of Tuvalu, 25.33 km^2 of land area are above MHWS. Funafuti, the most populous atoll of Tuvalu, has a maximum elevation

Table 2
Mean and Median Elevation and Land Area of Tuvalu's Islands Calculated From LiDAR Topography Data

Island name	Mean elevation above MSL (m)	Median elevation above MSL (m)	Mean elevation above MHWS (m)	Median elevation above MHWS (m)	Land area above MSL (km^2)	Land area above MHWS (km^2)
Funafuti	1.48	1.52	1.12	1.08	3.98	2.85
Nanumaga	2.52	2.35	1.96	1.64	2.83	2.48
Nanumea	1.96	1.98	1.33	1.22	3.94	3.46
Niulakita	3.26	3.47	2.75	2.86	0.46	0.42
Niutao	2.44	2.64	2.2	2.17	2.4	1.87
Nui	0.97	0.56	1.17	1.09	10.87	4.25
Nukufetau	1.44	1.53	1.06	1.01	4.34	3.11
Nukulaelae	1.15	1.13	1.06	1.03	3.52	1.91
Vaitupu	1.75	1.75	1.32	1.17	6.36	4.98
All	1.55	1.54	1.37	1.21	38.69	25.33

Note. Mean and median elevations and land area are provided in reference to mean sea level (MSL) and mean high water spring (MHWS).

of 6.93 m above MSL and a mean elevation of 1.48 m above MSL (1.12 m above MHWS). The atolls of Nukulaelae, Nukufetau, and Nui also have mean elevations <1.2 m above MHWS with median elevations <1.1 m. We compared the statistics obtained from the LiDAR survey to another commonly used topographic data set, that is, the Shuttle Radar Topography Mission (SRTM; Farr et al., 2007) data set. In the SRTM data set, the mean elevation above MSL in Tuvalu is overestimated by 7.65 m (>590%) while the maximum elevation is overestimated by 16.52 m (>250%). This highlights the inadequacy of coarse global data sets for coastal hazard assessments in low-lying small island nations and the need to invest in accurate baseline data.

3.2. Wave Hindcast

Wave data were obtained by performing a 44-year (1979–2022) hindcast of the wave conditions in Tuvalu using the unstructured version of the third-generation wave model Simulating Waves Nearshore (UnSWAN; Booji et al., 1996). The model is a Eulerian formulation of the discrete wave action balance equation (Booij et al., 1999). The computational mesh was generated using OceanMesh2D, a MATLAB based software package for two-dimensional unstructured mesh generation (Roberts et al., 2019). The spatial resolution of the flexible mesh ranged from 20 km offshore to 300 m around the atolls and in shallow waters. The grid domain covered the area between 11.5°S and 4.5°S and between 175.5°E and 178.5°W (12949 nodes/25269 elements).

The model was forced with 1-hourly 10 m surface winds and 1-hourly 2D wave spectra from the European Centre for Medium-Range Weather Forecasts (ECMWF) Reanalysis v5 (ERA5) (Copernicus Climate Change Service (C3S), 2017). A more detailed description of the model setup and validation is provided in Wandres et al. (2023).

3.3. Offshore Water Levels

3.3.1. Astronomical Tides

Tides around Tuvalu's nine islands were obtained from the well-established global tide model TPXO8 (Egbert & Erofeeva, 2002). Tidal elevations were extracted using the Tide Model Driver (TMD) MATLAB software package (https://github.com/EarthAndSpaceResearch/TMD_Matlab_Toolbox_v2.5) for the time period corresponding to that of the wave hindcast (1979–2022). A previous study by Hoeke et al. (2021) compared the skill of TPXO in Tuvalu against tidal predictions based on hourly tide gauge observations and found a good agreement between modeled and observation-based tides.

3.3.2. Mean Sea Level Anomalies

The computation of total water levels requires a seamless uninterrupted time series covering the same period as the wave hindcast and the tidal elevation time. Consequently, satellite measured sea surface heights were unsuitable as the time series only spans back to 1992. Hoeke et al. (2021) analyzed three global gridded sea level

Table 3
Increments for Projections of Sea Level Rise in Tuvalu Relative to the 1995–2014 Mean Sea Level

	Intermediate SSP2-4.5 (m)	Very high SSP5-8.5 (m)
2060	0.34	0.38
2100	0.73	0.91

Note. Values obtained from PRIF (2021).

products and evaluated their ability to reproduce non-tidal sea levels in Tuvalu and Kiribati. The authors found that the Ocean ReAnalysis System 5 (ORAS5; Zuo et al., 2019) monthly sea surface height reproduced the non-tidal residual most accurately compared to other sea level products. Hoeke et al. (2021) analyzed the residual sea surface height (observed water levels subtracted from predicted tides) variance at the Funafuti tide gauge and found that the median 30-day low-pass filtered variance is about 5–10 times larger than the high-frequency variance. This is typical in low-latitude Pacific locations, where seasonal and interannual phenomena (e.g., ENSO) dominate the sea level variability. The error introduced by neglecting higher-frequency sea level fluctuations (by choosing a monthly sea surface height product such as ORAS5) is therefore considered to be relatively small. ORAS5 sea surface height data were linearly interpolated to hourly time steps to match the wave hindcast. The mean sea surface height of the period between 1999 and 2009 was considered as mean sea level = 0 m.

3.3.3. Sea Level Rise Projections

Sea level rise projections were obtained from the Pacific Region Infrastructure Facility (PRIF) Guidance for Managing Sea Level Rise Infrastructure Risk in Pacific Island Countries Report (2021). The report compiles sea level rise projections for most Pacific Island Countries based on the Intergovernmental Panel on Climate Change (IPCC) 6th Assessment Report (AR6). Here we consider two socioeconomic pathways (SSP2-4.5 and SSP5-8.5) for two different time horizons (2060 and 2100). The sea level rise projections (Table 3) were applied assuming no geomorphological changes to the islands or reefs. Analysis of the Funafuti drill core collected by the Royal Society Coral Reef Expedition in 1896–1898 suggests the reef at Funafuti atoll grew upwards 26.4 m from 8 to 3 ka, indicating a Holocene vertical reef growth rate of ∼5 mm yr^{-1} (Ohde et al., 2002). In line with this, recent studies suggest that coral reefs islands have at least some capacity to keep up with sea level rise (e.g., Beetham et al., 2017; Duvat, 2018; Tuck et al., 2019). However, it is important to note that the processes which result in these natural physiographic changes (such as accretion during inundation events) themselves pose serious threats to life and infrastructure. When considering the natural adaptability of reef islands in the context of sea level rise, it is therefore necessary to separate the questions of (a) physical island persistence (e.g., can an island physically persevere when subjected to rising sea levels and increasing numbers of overtopping events) and (b) the ability of islands to sustain human life. Nevertheless, natural changes, combined with man-made coastal protection and climate change adaptation solutions, as well as anthropogenic development, mean that Tuvalu's bathymetry and topography will undoubtedly have changed by 2060 or 2100 and therefore the results of this study can be considered conservative.

4. Methodology

4.1. Overview

The methodology consists of a range of numerical and empirical models and processing steps (Figure 2). The underlying idea was to first generate large amounts of local extreme offshore ocean conditions considering waves, tides, and mean sea level anomalies. We distinguished between extreme wave conditions generated from distant sources and local tropical cyclones. The flooding potential during non-tropical storm conditions (regular conditions) is characterized by analyzing the dependence between wave parameters and sea level anomalies. Ten thousand years of synthetic extreme wave and water level conditions were produced using a Monte-Carlo simulation based on the 44-year national-scale high-resolution wave hindcast and sea level anomalies. To characterize TC driven inundation, three thousand years of TC activity were simulated by forcing the national-scale wave model with the parametric vortex wind fields from the TC tracks produced by the Synthetic Tropical cyclOne geneRation Model (STORM; Bloemendaal et al., 2020) data set. In a first pass, proxy total water levels (TWL_{Proxy}) nearshore were estimated empirically to perform an extreme value analysis of waves and water levels. Three combinations of wave parameters, sea level anomalies, and tide levels producing nearshore extreme water levels corresponding to proxy TWLs of particular return intervals were extracted. These were used to force a phase resolving numerical model, which in turn was used to generate probabilistic inundation maps.

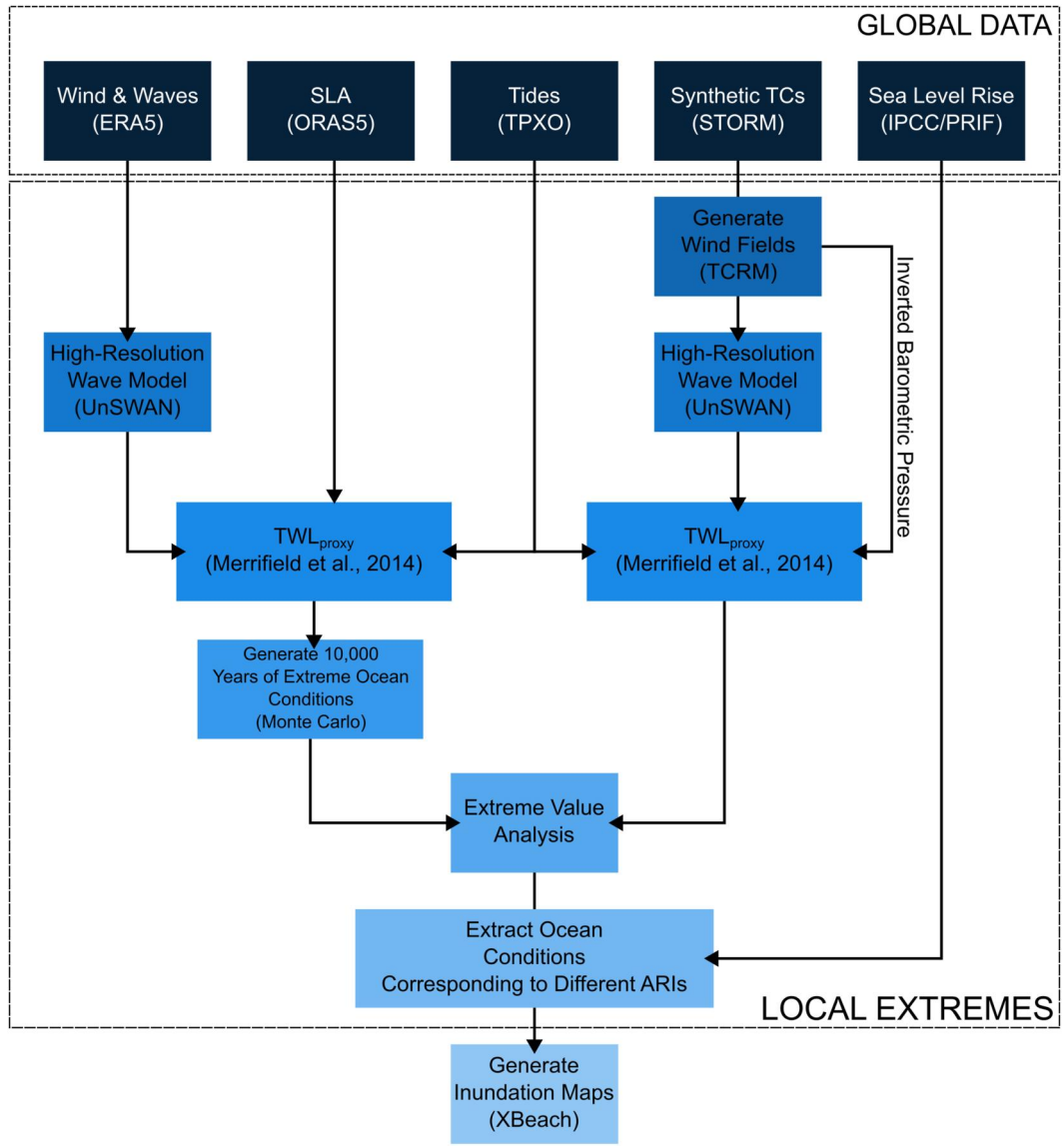

Figure 2. Flow-chart showing the methodology used to generate the probabilistic inundation hazard maps.

4.2. Regular Conditions

Wave-driven flooding results from the interaction of multiple oceanographic processes, where tides, mean sea level anomalies, and waves all interact to create an extreme total water level (TWL). As such, wave-driven floods are compound events. The main characteristics of a compound extreme event are: (a) the extremeness of the hazard rather than the individual component; (b) the multivariate nature of the hazard; and (c) the statistical dependence of the different components (Camus et al., 2017; Rueda, Camus, et al., 2016; Rueda, Gouldby, et al., 2016). Statistical models of coastal flooding often rely on parametric estimations of the extreme value distribution of each variable such as the generalized extreme value (GEV) or generalized Pareto distribution (GPD) and then, exploring the dependence between variables via copula functions (e.g., Izaguirre et al., 2010; Li et al., 2012; Méndez et al., 2007). However, these conventional methods fail to accurately reproduce return intervals in areas where the extreme events respond to different forcing mechanisms that generate statistically different populations or a mixed distribution (e.g., O'Grady et al., 2022).

Tuvalu's wave climate is dominated by three distinctly different sources: (a) long-period swells generated in the Southern Ocean and Tasman Sea, and in the North Pacific propagating through the South Pacific until reaching

Tuvalu; (b) locally, the prevailing trade winds responsible for short period easterly waves; (c) tropical cyclones in the low- and mid-latitudes, that can cause large waves, often from the west (Barstow & Haug, 1994; Bosserelle et al., 2015a; Hoeke et al., 2021; Wandres et al., 2023). In this context the use of non-parametric models such as the Kernel distribution is most appropriate (Rached & Larsson, 2019). Non-parametric mixture models have previously been used in fields such as economics (Zambom & Dias, 2012), health science (MacDonald et al., 2011), space science (Koons, 2001), climate science (Beranger et al., 2016), and oceanography (Boldi & Davison, 2007) as they avoid the specification bias implied by parametric estimators.

The methodology used to obtain the return intervals of the multivariate extreme events is comprised of five steps:

(1) Obtain a first order estimate of the nearshore total water level (TWL), that enables the selection of the combination of the variables responsible for coastal flooding.
(2) Fit of non-parametric covariance models (Kernel distributions) of the pairs of inundation drivers significant wave height (H_s), wave period (T_p), wave direction (θ_p), and mean sea level anomaly (MSLA).
(3) Generate 10,000 years equivalent number of synthetic extreme events.
(4) Estimate the return intervals of the nearshore TWL using a proxy empirical response function.
(5) Extract the inundation drivers (H_s, T_p, θ_p, *and MSLA*) corresponding to the different return intervals of the proxy empirical response function.

Empirical runup and overtopping estimates based on offshore ocean conditions and bathymetry and topography are well established (e.g., Franklin & Torres-Freyermuth, 2022; Gouldby et al., 2014; Liu et al., 2023; Merrifield et al., 2014; Stockdon et al., 2006). These formulations are widely used in coastal hazard, coastal engineering, and flood forecasting applications (e.g., Almar et al., 2021; Gouldby et al., 2014; Merrifield et al., 2021; Stockdon et al., 2023; Vitousek et al., 2017; Vousdoukas et al., 2018, 2023).

Here, a first estimate of the TWL nearshore was calculated as

$$TWL_{proxy} = \eta_{MSLA} + \eta_{tide} + \eta_2 \tag{1}$$

where η_{MSLA} and η_{tide} are the MSLA and tide respectively, and η_2 is the 2% exceedance water level nearshore described by Merrifield et al. (2014). η_2 is estimated as the exceedance level of continuously (1 Hz) sampled surface elevation with tides, mean sea level, and nonwave-related sea level anomalies removed. A linear dependence to derive η_2 is used:

$$\eta_2 = b_1 H_b + b_0 \tag{2}$$

where H_b is the breaker wave height

$$H_b = \left(H_s^2 T_p (4\pi)^{-1} \cos(\theta_p - \theta_N)\sqrt{\gamma g}\right)^{\frac{2}{5}} \tag{3}$$

where θ_N is the local shore-normal angle and γ is ratio of breaking H_b to breaking water depth, assumed to be ($\gamma = 1$) in line with Becker et al. (2014) and Vetter et al. (2010). Following Hoeke et al. (2021) who studied wave driven flooding in Tuvalu and Kiribati triggered by distant TC Pam, we assumed the two empirical coefficients to be $b_1 = 0.3$ and $b_0 = -0.1$. Note that due to the discrete nature of the wave peak period T_p, we used the mean period (T_m) to fit smooth statistical distributions. T_p was later estimated using the empirical relation of T_m/T_p, which was obtained from the 44-year hindcast.

We used the 95th percentile of the TWL_{proxy} peak-over threshold (POT) to choose the extreme values of H_s, T_p, and the *MSLA* (Figure 3). Note, that wave and water level conditions during the time of local TCs throughout the hindcast were omitted to avoid double-counting. See Section 4.3 for local TC conditions.

From each driver, the marginal distribution responsible for generating the proxy extreme TWL was fit to a nonparametric Kernel type distribution (Figure 4). The classical Kernel estimator approximates the probability Kernel density functions centered at each data point and then normalizes the sum to ensure a total probability mass of one (Rached & Larsson, 2019). Even though Kernel estimation is non-parametric with respect to the underlying distribution, the bandwidth parameter, which determines the smoothness of the density estimate needs to be

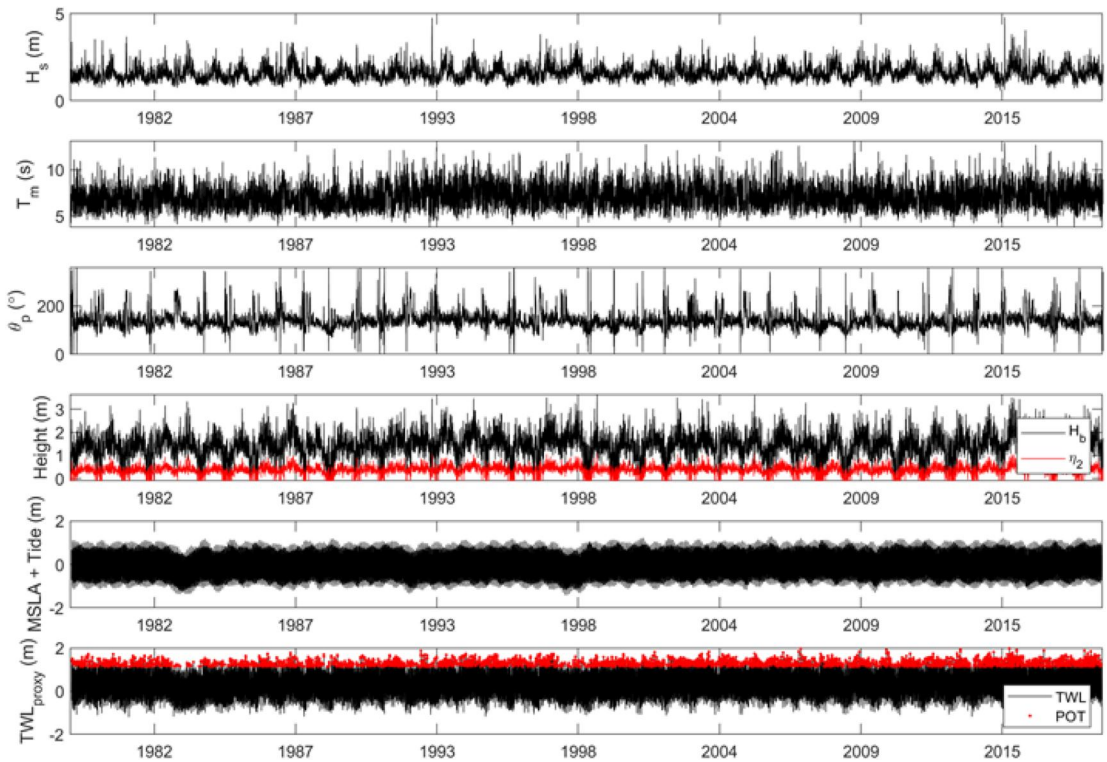

Figure 3. Time series of H_s, T_m, and θ_p from the UnSWAN wave hindcast used to calculate H_b and η_2 at an exemplary location south of Funafuti. η_2, MSLA and Tide level were used to calculate TWL_{proxy}. Red dots in the bottom panel identify selected extremes exceeding the 95th percentile of the TWL_{proxy}.

chosen. Here, the Improved Sheather-Jones bandwidth selection algorithm was used, with no assumptions on the true distribution. This bandwidth selector has been shown to perform well for non-normal distributions. An example of the discrete marginal distributions and Kernel density plots for H_s and T_m and for H_s and MSLA are shown in Figure 4.

To incorporate the wave direction as one additional covariate into the model, the smoothed empirical distributions of direction were determined for each 0.25 m interval of H_s (Figures 4e and 4f). For the higher percentiles of H_s, the obtained relation was extended to 1.5 times the maximum value of the H_s contained in the marginal distribution. Then the obtained irregular surface was smoothed to guarantee an even transition of the wave direction distribution for every wave height interval (Figure 4f).

Once the marginal distributions and the dependence structure between variables were fit, it was possible to generate synthetic extreme oceanographic conditions that have the potential to inundate coastlines. Knowing the rate of occurrence of these extreme conditions in the historical record (number of exceedances of the first guess TWL in a time block) and considering stationarity in the process, we generated 10,000 years of plausible extreme events (Figure 5). Using the 10,000 years of extreme wave conditions and offshore water levels, we then calculated 10,000 years of synthetic extreme nearshore TWL_{proxy} using Equation 1 (Figure 6). The 10,000 years of extreme nearshore TWL_{proxy} values were resampled to 25,400-year blocks (bootstrapping) to calculate return intervals and 95% confidence intervals (Figure 7). We considered the occurrence of extremes to be independent of tidal drivers. We therefore added a randomized tidal signal (η_{tide}) to each of the extreme events.

4.3. Tropical Cyclone Conditions

The previous section describes the development of 10,000 years of synthetic extreme ocean conditions. However, the synthetic database still depends on the underlying forcing conditions, namely, wind and boundary wave conditions from ERA5 between 1979 and 2022. While global wind and wave models perform well in describing average wind and wave climate, they are known to under-predict extreme wind and wave events such as tropical cyclones (TCs) (e.g., Appendini et al., 2013; Murakami, 2014). Particularly rare extreme cyclones are therefore

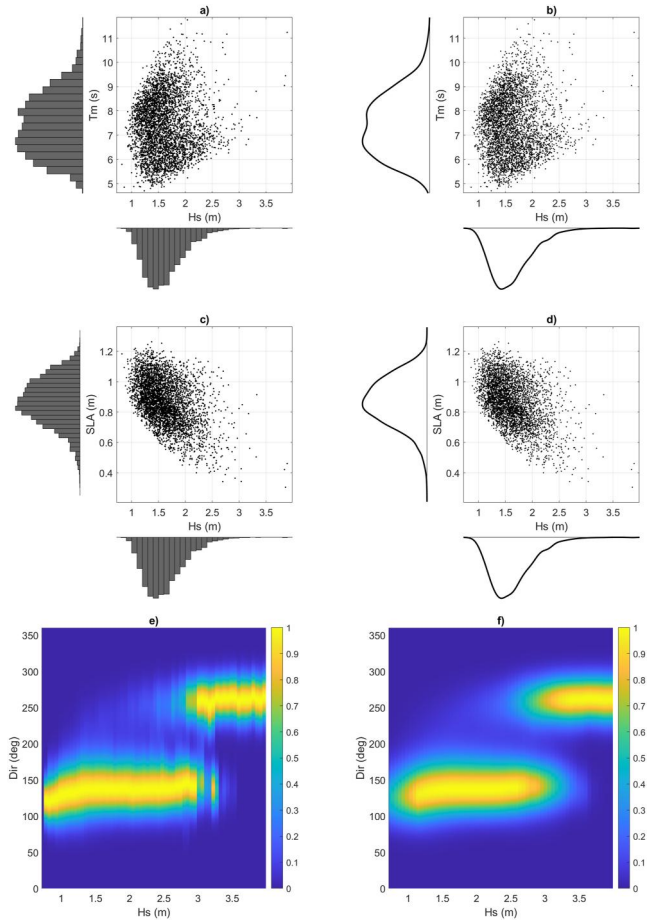

Figure 4. Scatter plots and (a and c) marginal histograms and (b and d) kernel density plots, displaying the relationship between H_s and T_m (a and b) and H_s and SLA (c and d). Distribution and smoothed distribution (probability density) between H_s and θ_p are displayed in (e) and (f) respectively.

not well captured. According to the International Best Track Archive for Climate Stewardship (IBTrACS), only 5 TCs between category 1–5 crossed within 150 nautical miles of Funafuti, three of which occurred before 1979 and are therefore not included in the wave hindcast. However, while Tuvalu can be subject to flooding from distant TCs such as TC Pam in 2015 (Hoeke et al., 2021) it can also be impacted by severe local TCs such as TC Bebe in 1972 (Maragos et al., 1973). Local TCs should therefore also be considered in coastal flood hazard assessments. In a recent paper Bloemendaal et al. (2020) developed a synthetic resampling algorithm called Synthetic Tropical cyclOne geneRation Model (STORM) and used it to generate 10,000 years of synthetic TCs based on 38 years of historical TC data from the IBTrACS database.

The STORM database provides 3-hourly TC tracks (latitude and longitude), minimum TC pressure, maximum wind speed, and radius to maximum wind speed (RMW) for each TC (Bloemendaal et al., 2020). We extracted the TC tracks from the STORM database that crossed through the area between a longitude of 168°E and 162°W and between a latitude of 18°S and 1°N. TCs outside this domain were considered distant TCs that should be captured by the method outlined in Section 4.1. Wind fields for each TC track were reconstructed using the parametric wind field generator of the Tropical Cyclone Risk Model (TCRM; Arthur, 2021). We used the default model parameters following Arthur (2021). The Powell et al. (2005) wind profile, a variant of the Holland (1980) wind profile, was applied, where the peakedness parameter (β) was defined as

$$\beta = 1.881093 - 0.010917|\lambda| - 0.005561R_{max} + \varepsilon \quad (4)$$

where λ is the latitude of the TC center and ε is a random variate sampled from a normal distribution with zero mean and a standard deviation of 0.286 (Arthur, 2021; Powell et al., 2005). The boundary layer model of Kepert (2001) was applied to relate gradient level winds to those near the surface.

The synthetic TCs were validated against historic TCs. Historic (1970–2018) TC tracks were obtained from the Southwest Pacific Enhanced Archive for Tropical cyclones (SPEArTC; Diamond et al., 2012). The SPEArTC database includes 6-hourly track information (3-hourly intervals close to landfall) of the location (latitude and longitude) of the TC center, maximum 10-min averaged winds, and central pressure. RMW is required to reconstruct the parametric wind fields (Arthur, 2021) but not provided in the database. We therefore calculated the RMW of each TC using the empirical equation of Knaff et al. (2016), where

$$\mathrm{RMW} = 218.3784 - 1.2014V_m + \left(\frac{V_m}{10.9844}\right)^2 - \left(\frac{V_m}{35.3052}\right)^3 - 145.5090\cos\lambda \quad (5)$$

where V_m is the maximum wind speed in knots and λ is the latitude in degrees. After calculating the RMW we reconstructed the wind fields using the parametric wind field generator in TCRM (Arthur, 2021). A comparison of the histograms of SPEArTC and STORM minimum pressure (P_{min}), maximum wind speeds (V_{max}), and RMW (R_{max}) shows a good agreement between the historic and synthetic data sets (Figure S1 in Supporting Information S1).

The UnSWAN model was set up (same model grid as in Section 3.3) to simulate the wave conditions of the synthetic TC database (STORM) as well as the historic TCs (SPEArTC) locally affecting Tuvalu. Model settings were mostly the same as in Section 3.3, however, the wind drag formulation of Zijlema et al. (2012) was applied. This wind drag formulation has been found to be better suited for high winds speeds compared to the default

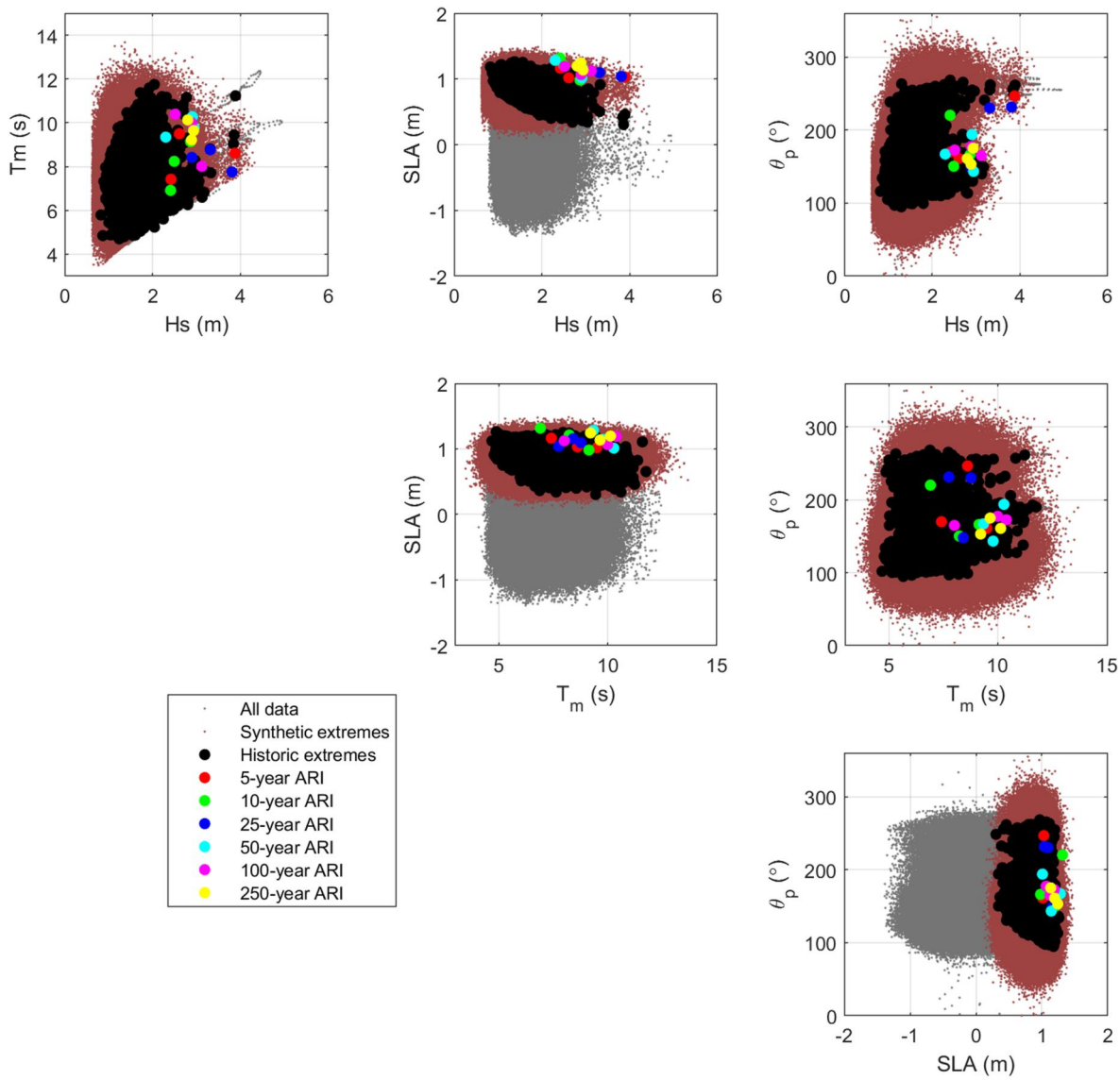

Figure 5. Scatter plots showing relationships between H_s, T_m, θ_p, and SLA. Gray dots display historic data, black dots indicate historic extremes, and red dots indicate the 10,000 years of synthetic extremes generated with the Monte-Carlo simulation. Colored dots indicate selected combinations of H_s, T_m, θ_p, and SLA for corresponding to different annualized return intervals (ARIs).

SWAN wind parameterization, which overestimates the wind drag in storm conditions (Zijlema et al., 2012). Hourly bulk wave parameters (H_s, T_p, T_m, θ_p, and θ_m) were stored at every point of the grid and directional wave spectra were stored around the islands. To validate the STORM database we compared the ARIs of H_s across the model domain against historic wave heights from the SPEArTC data set (Figure S1 in Supporting Information S1). The analysis showed an overall good agreement of synthetic extreme H_s (STORM database, black lines) compared to the historic database (SPEArTC, red dots), with only a few outliers in the high return intervals. Simulated wave conditions were used to calculate η_2 (using Equation 2).

As in Section 4.2, we estimated proxy total water levels (TWL_{proxy}) for each synthetic TC using Equation 1. In islands with narrow fringing reefs, wind setup can generally be neglected, as extreme water levels are dominated by the pressure deficit of TCs (Joyce et al., 2019; Tu'uholoaki et al., 2023). The sea level anomalies and storm surges (η_{MSLA}) were approximated with the inverse barometer effect where 1 hPa drop in atmospheric pressure corresponds to 1 cm increase in SLA. We considered TC occurrence to be independent of tidal drivers. We therefore added a randomized tidal signal (η_{tide}) for the duration of each TC. The tidal signal was generated using a

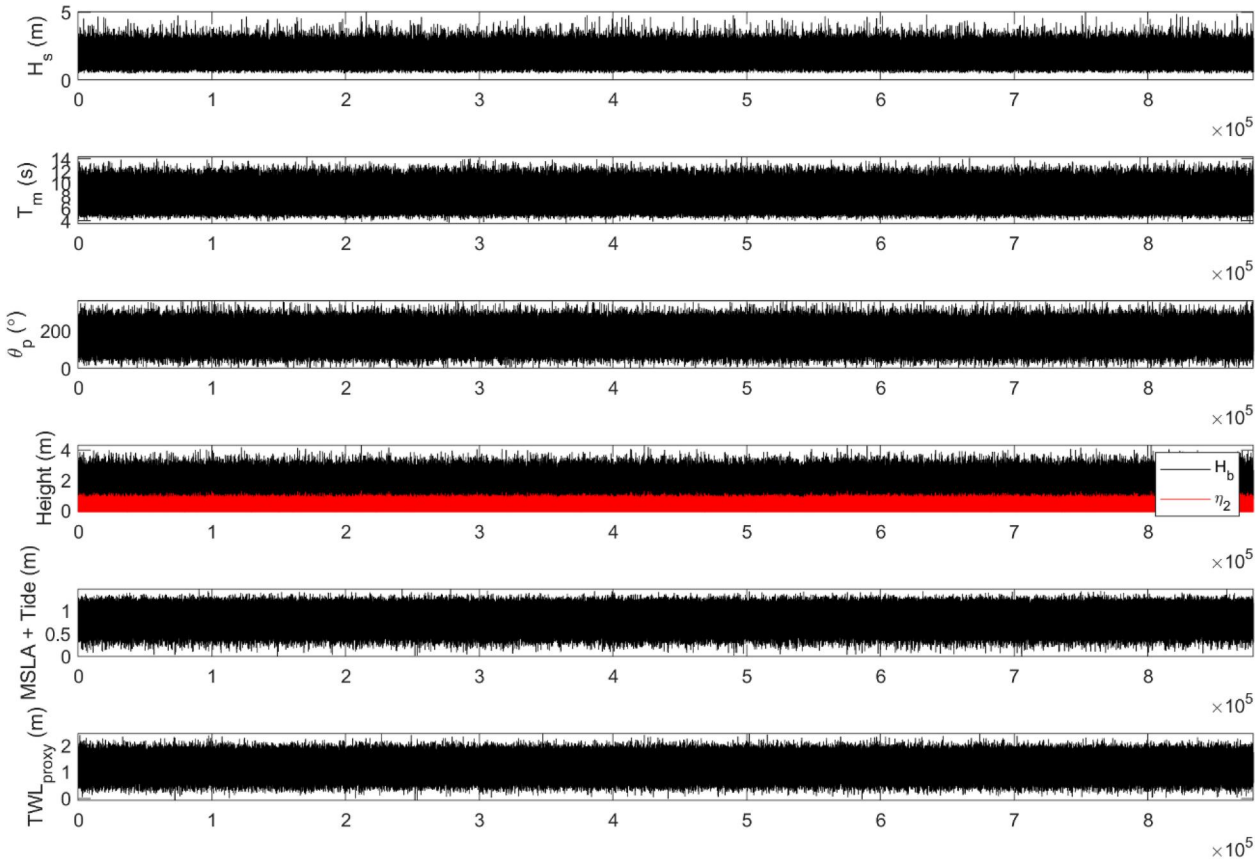

Figure 6. 10,000 years of extreme H_s, T_p, θ_p, H_b, and η_2, offshore water level ($\eta_{MSLA} + \eta_{tide}$), and proxy TWL near the shore in Funafuti under present MSL.

random starting time and calculating a time series of tidal elevations using TPXO8 at the location of the TC. TWL_{proxy} of TCs were sorted by magnitude and resampled using the bootstrapping method (see Section 4.1) to determine return intervals (Figure 7). Note that while the STORM database provides 10,000 years of TCs, the extreme value analysis of the TC generated waves and TWL_{proxy} indicated a convergence of the return intervals between 5 and 250 years after ~2,000 years of simulations (i.e., return intervals of TWL_{proxy} and wave conditions for the considered ARIs did not change significantly after 2,000 years of TCs were considered). However, to stay on the conservative side, whilst maintaining a feasible computational expense, we obtained TC tracks of the first 3,000 years rather than using the entire 10,000-year database.

5. Flood Simulations

Wave driven inundation usually occurs as a compound event of tides, sea level anomalies, and non-linear wave transformation processes. The wave transformation processes consist of breaking wave induced setup, infragravity waves, and waves in the sea-swell frequency band. We simulated the compound events corresponding to the 5-, 10-, 25-, 50-, 100-, and 250-year annual recurrence intervals of TWL_{proxy} (see Section 4) using the numerical model XBeach (Roelvink et al., 2009) in non-hydrostatic (NH) mode. XBeach is a coupled circulation and wave model that resolves the wave transformation including swash hydrodynamics (e.g., infragravity waves) using the non-linear shallow water equations. In non-hydrostatic mode, dispersive waves are simulated using a depth-average flow model with a similar accuracy yet reduced computational expense to that of lower-order Boussinesq models (Smit et al., 2010). The model has been shown to accurately reproduce wave transformation in coral reef environments (e.g., Klaver et al., 2019; Lashley et al., 2018; Pearson et al., 2017).

Our methodology to generate the flood maps follows Storlazzi et al. (2019) who evaluated the role of coral reefs in reducing coastal hazard risk. This was done by propagating offshore wave and water level conditions across shore-normal transects using XBeach and then interpolating the maximum water levels between the transects to

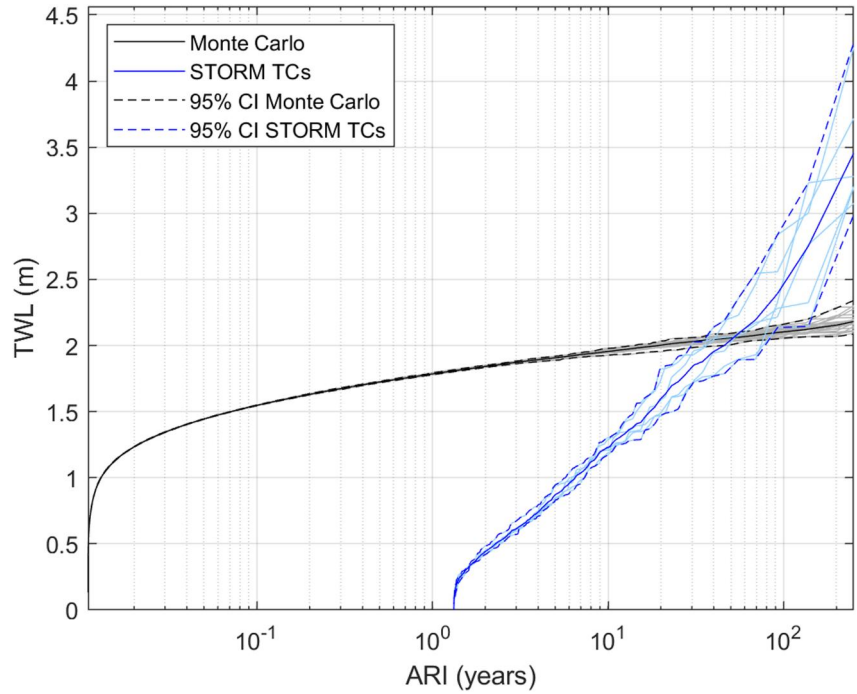

Figure 7. Annualized return intervals (ARIs) for nearshore TWL_{proxy} at an exemplary location south of Funafuti derived from 10,000 years of synthetic extreme ocean conditions generated with a Monte-Carlo simulation (black line); and for 3,000 years of tropical cyclone conditions based on the STORM database (blue line). Striped lines indicate 95% confidence intervals.

produce flood maps. The application of 1D models neglects some of the hydrodynamic processes that occur on natural coastlines (e.g., long-shore currents). However, since the directional output from the high-resolution SWAN wave model, which the XBeach forcings are based on, indicates predominantly near-normal wave conditions near the coastline, a 1D modeling approach is justified (e.g., Storlazzi et al., 2019). Since IG and short-wave energy are propagated shore-normally across the 1D XBeach domain, and incoming wave energy might therefore be slightly over-estimated (e.g., Roelvink et al., 2018), our approach can overall be considered conservative. However, the extent of flooding might be slightly underestimated in areas with protruding land formations, where the convergence of wave energy leads to heightened wave-driven flooding that cannot be adequately predicted using one-dimensional models (e.g., wave focusing). Similarly, the impact of wave-driven flooding is likely underestimated in small bays and inlets where wave energy is dispersed through diffraction.

The bathymetry and topography cross-shore transects were extracted every 100 m around each island (Figure 8). The ocean side of each transect extended into deep waters >50 m. XBeach transects were forced with wave parameters and water levels from the extreme value analysis (Section 4), obtained for each one of the transects. To obtain forcing, the 5-, 10-, 25-, 50-, 100-, and 250-year annual recurrence intervals TWL_{proxy} were established for synthetic TC conditions (blue line in Figure 7) and regular conditions (black line in Figure 7), and the larger value was chosen. Combinations of water levels ($\eta_{tide} + \eta_{SLA}$) and wave conditions (H_s, T_p, θ_p) corresponding to a certain TWL_{proxy} were then extracted as boundary forcing for the XBeach simulations. Individual waves and wave groups within a sea state are somewhat random. Consequently, simulating a certain sea state in nonhydrostatic mode will yield slightly different results each time, unless the model is run for a long time in a quasi-stationary simulation. To reduce the simulation time, three simulations per return interval (with three different sets of forcings corresponding to each return interval, see Figure 5 as an example) were run. This allowed us to increase the variability of the sea state, while maintaining the corresponding runup through the multivariate mapping using Equation 1 and consequently improving the accuracy of the flood simulations while reducing simulation times to 90 min per run. The multi-model mean of the inundation extent and depth of the three simulations was used. Such an event-based approach to determine flooding has the advantage that only a relatively small number of design events needs to be simulated and future changes (e.g., SLR) can simply be incorporated, assuming that the

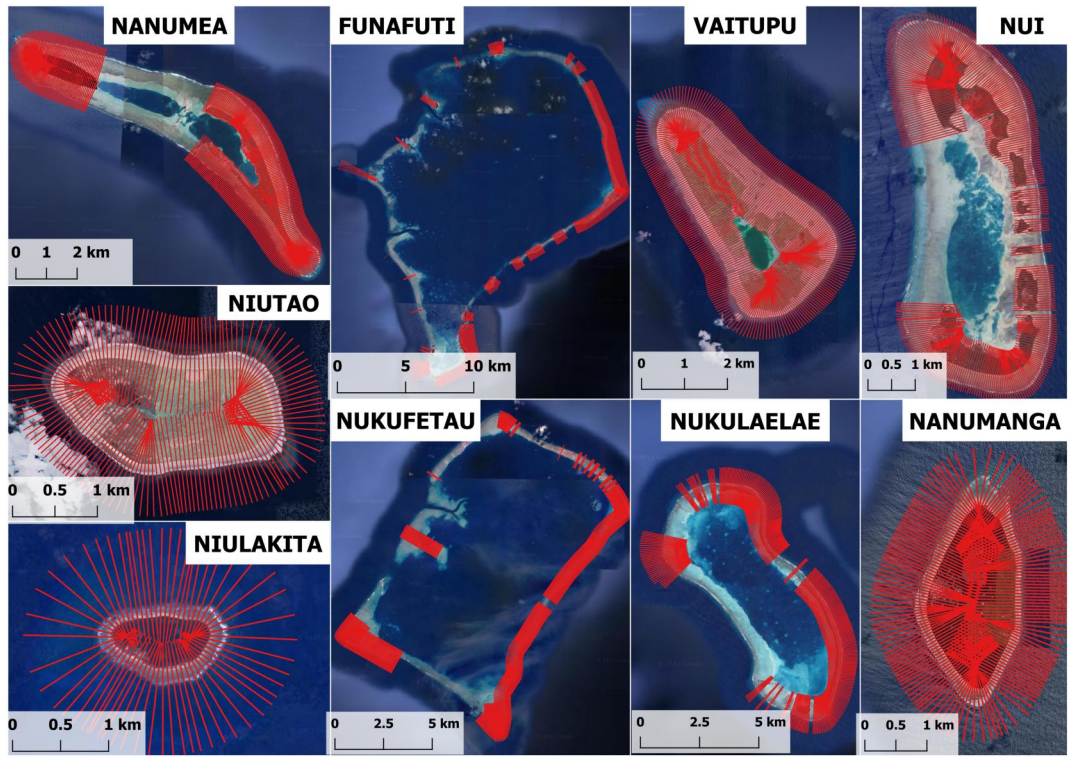

Figure 8. Cross-shore transects used for the XBeach NH simulations.

dependencies between variables are unaffected by the change. The drawback of this approach is that temporal and spatial dynamics can become lost (Wu et al., 2021). However, since we are concerned with wave-driven flooding on reef-fronted islands, temporal dynamics can be considered negligible (i.e., wave-driven flooding occurring now is largely unaffected by the wave conditions of the previous day and all relevant temporal effects are resolved in our XBeachNH simulations). Our method accounts for spatial variability as separate extreme value analyses are performed every 100 m. For example, the 25-year ARI flooding on one side of an island might be caused by waves generated by a TC while the 25-year ARI flooding on the other side of the island might be caused by a combination of waves and extremely high tides.

In Figure 7 it can be seen how for low ARIs, TWL_{proxy} is dominated by regular (non-cyclonic conditions) resulting from the Monte Carlo simulation, while higher ARIs (e.g., >52-year ARIs), result from the synthetic TCs (for an exemplary transect south of Funafuti, Figure 7). TWL_{proxy} were re-computed for the different SLR scenarios (Table 3) and the different return intervals were simulated for the various future scenarios. Each simulation was run for 90 min, to allow a 30-min spin-up while the free surface elevation (z_s), maximum free surface elevation ($z_{s,max}$), and current velocities were stored for the following hour. The maximum inundation was calculated as $z_{s,max} - z_b$, where z_b is the bed level (i.e., bathymetry and topography).

Total water levels along the shore-normal transects were then interpolated onto a ~5 m by 5 m grid to produce flood maps following Storlazzi et al. (2019). The interpolated surfaces were smoothed to remove interpolation artifacts. The inundation surface was then subtracted from the DEM. In this analysis we only considered flood depths ≥0.1 m, as these exceed the range considered as nuisance flooding as defined in Moftakhari et al. (2018). Areas with values ≥0.1 m were considered inundated while values <0.1 m were considered dry. Hydraulic connectivity was checked to avoid flooding in enclosed troughs not connected to the ocean.

In 2013, SPC deployed an array of oceanographic sensors off the coast of Fatato, one of Funafuti's islets (Beetham et al., 2016; Bosserelle et al., 2016). The survey included an offshore wave sensor at approximately 20 m depth off the reef and two pressure sensors on the reef crest and nearshore respectively. Both were sampling the free surface water elevation 3-hourly at 2048 s long 1 Hz bursts. A more detailed description of the study and instrument setups can be found in Bosserelle et al. (2016) and Beetham et al. (2016). To validate XBeach, we simulated a 15-

day period (1st October–15th October 2013) of the cross-reef transect where the instruments were deployed. This period featured two medium wave events ($H_s > 1.5$ m). XBeach was forced with incident wave heights, periods, and water levels from the offshore sensor (assuming shore-normality of the incident wave directions) and validated against the sensors on the reef flat and nearshore. The model was able to accurately simulate the observed wave heights (IG and waves in the sea swell frequency bands) with high correlation coefficients (>0.7) and low errors and biases. See Table S1 in Supporting Information S1 for detailed error metrics.

Due to a lack of appropriate in situ extreme wave and overtopping data, a scaled physical experiment was undertaken by the Water Research Laboratory (WRL) at the University of New South Wales (UNSW), Australia. A physical model of a representative cross-shore profile of the atoll of Nanumaga was constructed at a 1:25 scale, where the scaling relationship between length and time was determined by Froudian similitude (Blacka & Deiber, 2021).

Four experiments with extreme wave and water level conditions ($H_s > 5$m) were performed in the physical model (see Table S2 in Supporting Information S1). H_s and wave setup η_{mean} were recorded in the wave flume using seven wave gauges along the transect. Overtopping rates were also recorded. An XBeach model of the same cross-shore profile was created, and a multivariate sensitivity analysis was performed to fine-tune the numerical model parameters (e.g., Oliveira et al., 2020; Wandres et al., 2020). A comparison between the numerical and physical models of experiment 4 is shown in Figure S2 of the Supporting Information S1. Mean errors of H_s, η_{mean}, and overtopping rates of all experiments are provided in Table S2 of the Supporting Information S1. XBeach was able to accurately reproduce water levels (η_{mean} mean error of 0.46 m across all gauges and experiments), wave heights (H_s mean error of −0.03 m across all gauges and experiments), and overtopping rates (mean error of −0.6 l/s/m across all experiments).

Simulated flood extents and depths were qualitatively validated against flood maps produced by the Tuvalu Government Public Works Department during a post-disaster survey after distant TC Pam in 2015. Overall, the models were able to reproduce inundation extents of TC Pam well. For example, certain roads and houses marked as inundated by the Tuvalu Government Public Works Department were also inundated by the XBeach simulations (Figures S3–S9 in Supporting Information S1).

6. Results

This study presents a novel approach to determine the probabilistic hazard of coastal flooding in reef-fronted islands. By determining a TWL_{proxy} nearshore for TC conditions and for regular conditions we were able to determine combinations of wave and offshore ocean water levels responsible for extreme TWL nearshore and consequently flooding for different ARIs. Figure 9a shows the ARI at which local tropical cyclones dominate the nearshore TWL_{proxy} (i.e., the intersection between TWL_{proxy} ARIs of the regular climate and local TCs). The southernmost islands Nukulaelae and Niulakita, are most frequently exposed to local TCs, with TWL_{proxy} along their north coasts being dominated by TCs at ARIs ≤ 25 years. Funafuti's nearshore TWL is dominated by local TCs approximately every 30–60 years while Nukufetau's TWL_{proxy} is dominated by local TCs every ∼40–80 years. Due to the proximity to the equator and an inherent rarity of local TCs, northern islands are less affected by local TCs than the southern islands. Water levels in the northern islands are almost exclusively dominated by the regular conditions (ARIs ≥ 100 years) as TCs generally form and pass far south of these islands. Figures 9b–9f display the TWL_{proxy} for 10-, 25-, 50-, 100-, and 250-year ARIs respectively. Unsurprisingly, islands exposed more frequently to local TCs (e.g., Nukufetau, Funafuti, Nukulaelae, and Niulakita) also experience larger nearshore TWLs compared to the northern islands. TWL_{proxy} are generally larger (for ARIs < 100 years) on the western side of each island, with islands in the northern group experiencing the highest water levels in the south-west and islands in the southern group experiencing the highest water levels in the north-west. Due to the larger exposure to TC-generated swells/waves that tend to intensify over the warm waters of the southeast Pacific, higher return intervals (i.e., 250 years) showed bigger water levels in the north northeast of Funafuti and Nukulaelae. By investigating the contribution to the TWL_{proxy} from the different drivers it was shown that waves generally contributed to >50% of the total water level (with the remaining water level attributed to tides and sea level anomalies). The influence of waves increased in higher return intervals. By analyzing the wave periods corresponding to the TWL_{proxy} it was shown that distant-source swells (i.e., $T_p \geq 13$s) dominate flooding during the regular climate conditions. However, it should be noted that these could be originating from distant tropical or extra-tropical storms.

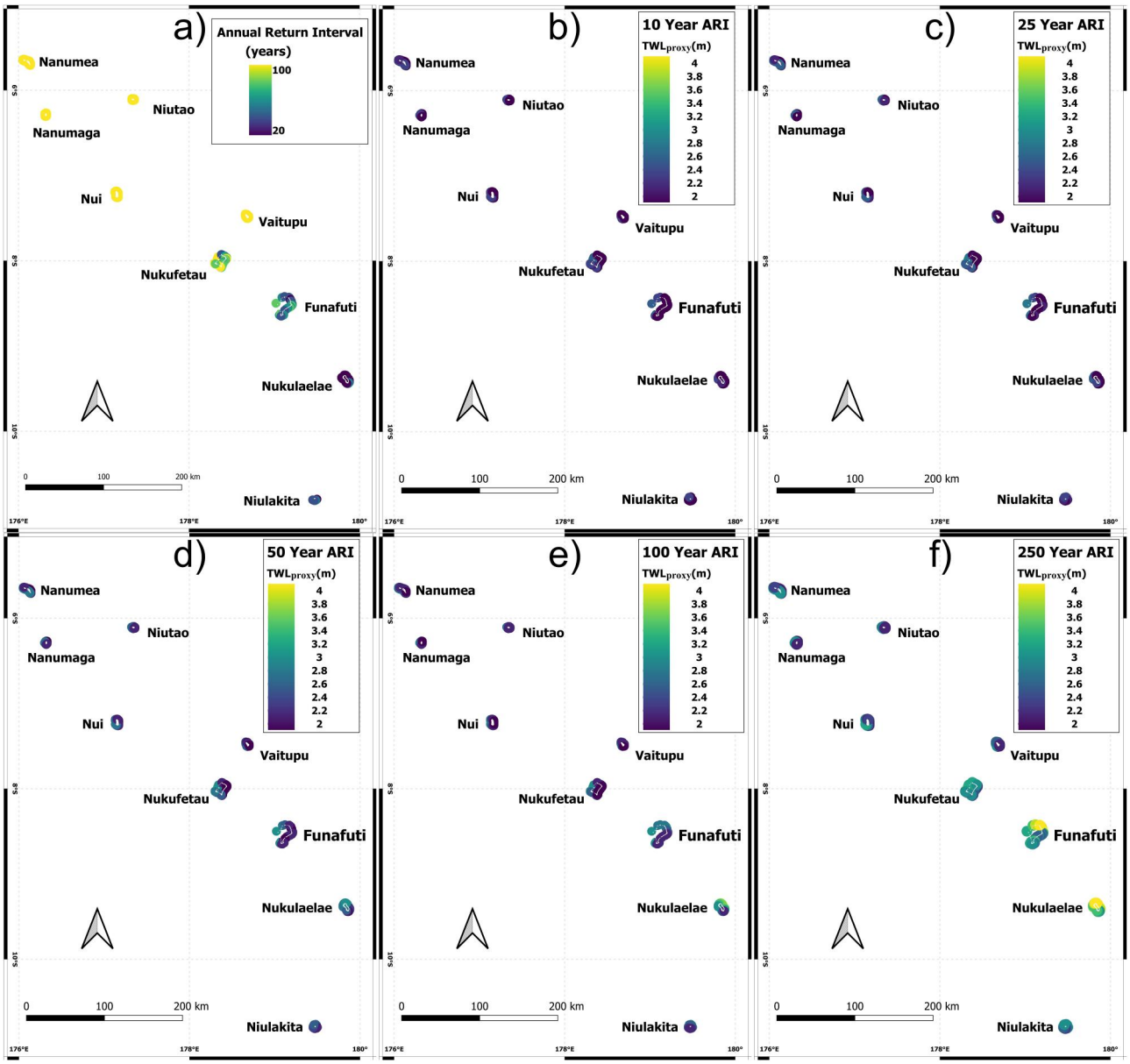

Figure 9. (a) Annual return interval (ARI) where TWL_{proxy} ARI from tropical cyclones exceeds that of the regular climate. (b–f) TWL_{proxy} for 10-, 25-, 50-, 100-, and 250-year ARIs respectively.

The flooded area above MHWS was calculated for each return period and sea level scenario (Figure 10). Under present sea levels ~6.9 km^2 (~27.2%) of land area inundate once every 5-year across all of Tuvalu. This value almost doubles to ~13.5 km^2 (~53.1%) for an ARI of 100 years. However, some islands are more likely to experience flooding than others. For example, it is well known that Funafuti experiences multiple floods annually due to spring tides, even in the absence of large waves or mean sea level anomalies. The porosity of the carbonate reef-borne ground results in a strong hydraulic connectivity between the ocean and Funafuti's interior (e.g., Patel, 2006; Webb, 2007; Yamano et al., 2007). This results in spring high tides penetrating the island from the ground up, without the need of wave overtopping. Furthermore, much of Funafuti's islets are extremely narrow (<100 m wide). Consequently >50% of the atoll area floods once every 10 years due to a combination of perigean spring high tides (king tides) and waves. Other islands such as Niutao and Niulakita are less frequently and extensively flooded. Only ~17% of the Niulakita's land area and only ~11% of Niutao's land area floods once in

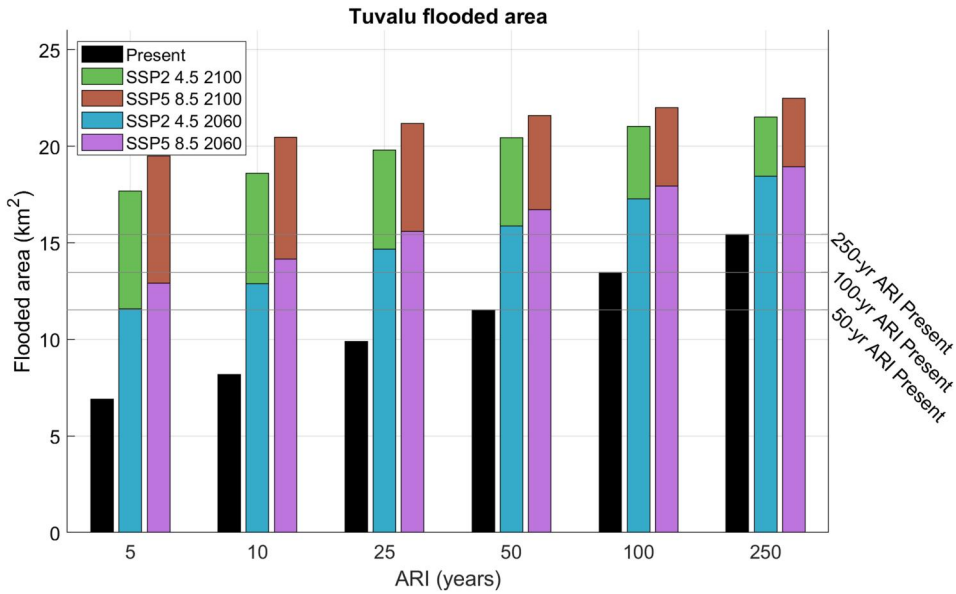

Figure 10. Flooded area above MHWS across all of Tuvalu for different annual return intervals (ARIs) and sea levels. Colors represent different sea level scenarios. 50, 100, and 250-year ARIs under present sea levels are highlighted by gray lines to ease comparison.

10 years (Figure 11). This is particularly interesting since Niulakita experiences higher TWLs and more frequent local TCs than the other islands (Figure 9). The reason for the reduced flood susceptibility lies in the islands' geomorphology as they are significantly higher than the rest of Tuvalu (>2.4 m above MSL, Table 1).

With sea level rise, the frequency of present-day rare extreme floods is projected to increase. For example, present-day 50-year ARI flooding becomes <5-year ARI flooding by 2060, even under the optimistic SSP2 4.5 sea level rise projections (Figure 10). Under the same scenario by 2100, 250-year ARI flooding is projected to occur more frequently than once every 5 years. Under the more pessimistic SPP5 8.5 scenario, flooding is projected to become even more extreme and frequent (Figure 10).

Figures 11a–11c show inundation maps for the inhabited area of Nanumea for 5-year ARI flooding under present sea levels (a), 50-year ARI flooding under present sea levels (b), and 5-year ARI flooding under the SSP2-4.5 2100 SLR projection (c). The red shaded area indicates the area where the inter-ensemble variability is >25% of the ensemble mean inundation depth, that is, areas with lower confidence in the model results. Further inundation maps for other return intervals for the present and SSP2 4.5 2100 sea levels are provided in Figures S10 and S11 of the Supporting Information S1. It is shown that the largest variability among the three ensemble members (red shading) is in areas where inundation is relatively low, indicating that these areas of uncertainty should not limit the usefulness of the results. Once every 5 years (Figure 11a), 29.6% of Nanumea's landmass become inundated, while 59.4% of the atoll become inundated once every 50 years (Figure 11b). By 2060 52.7% of the atoll's land mass will flood once in 5 years (under SSP2 4.5 SLR projections); and by 2100 81.4% of the area will inundate (Figure 11c) once every 5 years (under SSP2 4.5 2100 SLR projections). Figure 11d shows the return intervals at which certain areas of Nanumea are flooded during present sea levels. By 2100 (SSP2 4.5 projections) it is estimated that many areas presently only flooded once every 50, 100, or even 250 years, will flood once every 5 or 10 years (Figure 11e).

While there are differences across the various islands, the overall trends and timelines remain similar. In Funafuti, Nui, Nukufetau, and Vaitupu, present-day 50-year ARI flooding will become more frequent than 1-in-5-year by 2060 (Figure 12). In Nanumaga, Nanumea, Niutao, and Nukulaelae present day 50-year ARI flooding will occur more than once every 10 years by 2060, even under the more optimistic SSP2 4.5 SLR scenario (Figure 12).

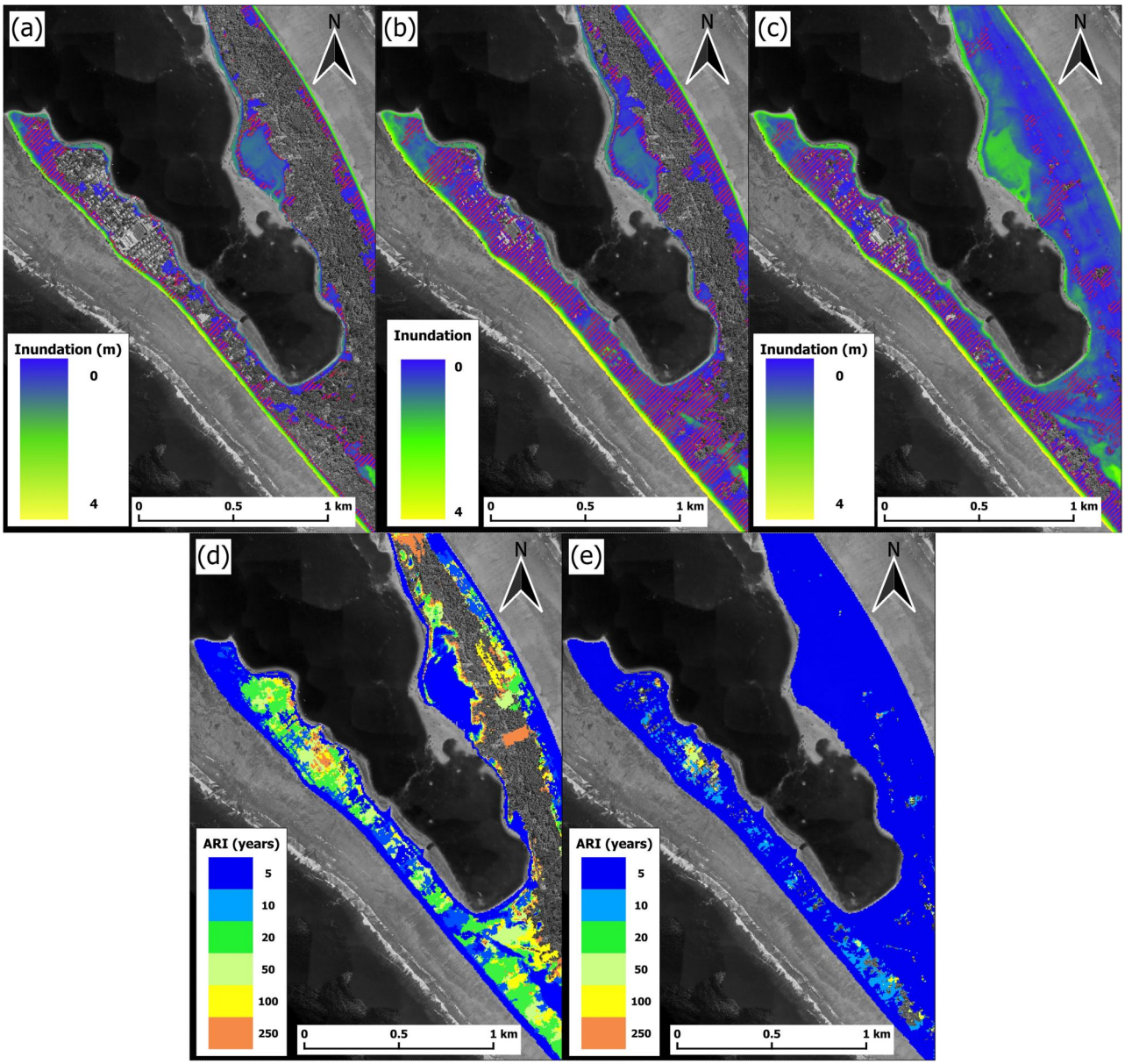

Figure 11. (a–c) Inundation maps for the main village in Nanumea. (a) 5-year ARI inundation at present sea level, (b) 50- year ARI inundation at present sea level, (c) 5-year ARI inundation with SLR corresponding to the SSP2-4.5 scenario (2100 time slice). Red shaded area indicates where the range of variability of the three simulations is smaller than 25% of the inundation depth. (d) Return intervals at which certain areas of Nanumea are flooded (under present sea levels). (e) Return intervals at which certain areas of Nanumea are flooded (under SSP2 4.5 projections of 2100 sea levels).

7. Discussion and Conclusion

This paper presents a novel and comprehensive methodology to address coastal inundation hazard in reef-fronted islands in the tropical Pacific across a wide range of scales. Here, we apply the methodology to the atoll nation of Tuvalu, leveraging on recently collected LiDAR topography and bathymetry data. Our methodology accounts for tides, mean sea level anomalies, and storm surges, along with a mixed climate (e.g., cyclone and non-cyclone wave conditions). Shallow water processes such as wave breaking and wave transformation across the reef flats are also considered. Hazard maps (inundation extent and depths) for different return periods were calculated for the present sea level and future SLR scenarios according to the latest IPCC Assessment Report (AR6). Results indicate that Tuvalu is highly susceptible to coastal inundation, with >25% of the nation flooded once every

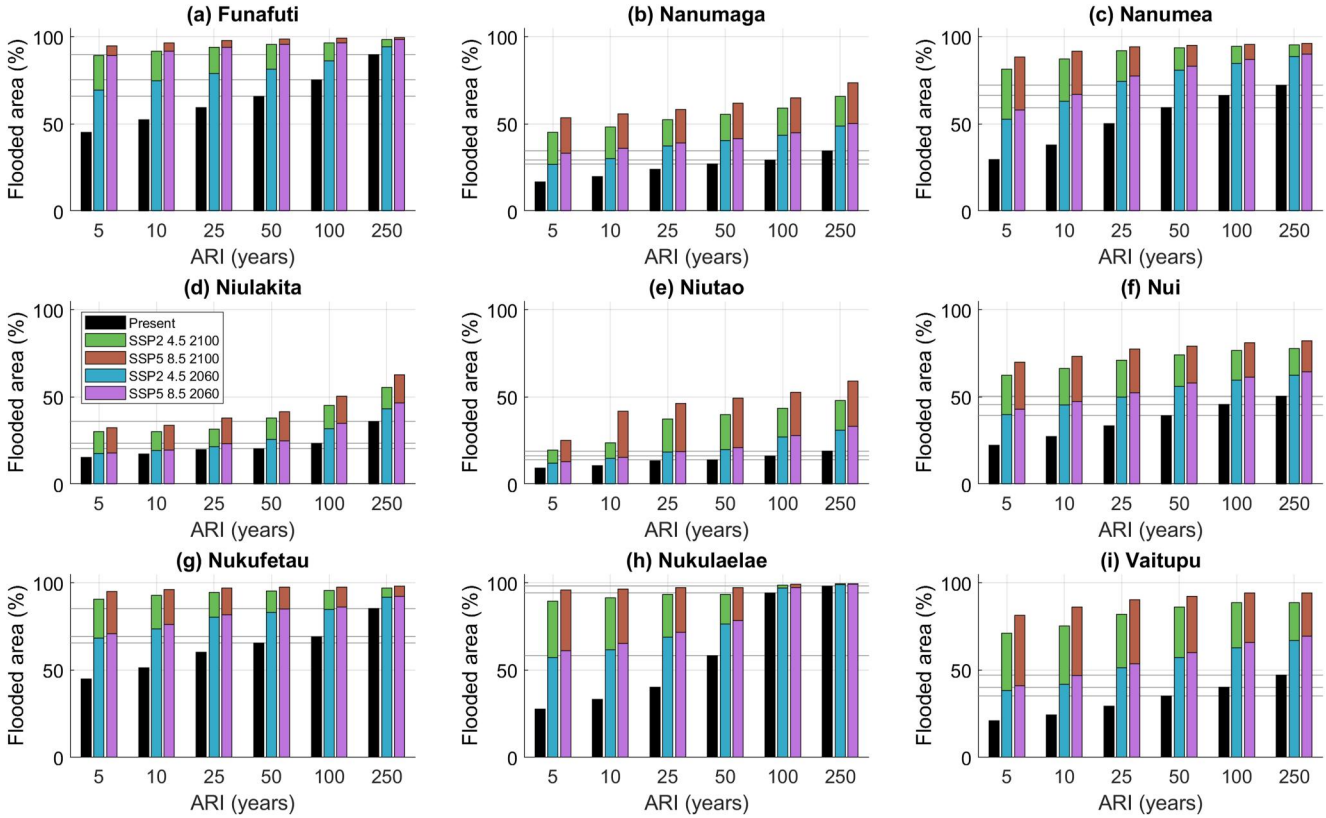

Figure 12. Percentage of flooded area above MHWS for different annual return intervals (ARIs) and sea levels for the different islands. As in Figure 10, 50, 100, and 250-year ARIs under present sea levels are highlighted by gray lines to ease comparison.

5 years. Present day 1-in-50 years floods (>45% of the nation flooded) will occur more than once every 5 years by 2060, even under the moderate SSP2 4.5 sea level rise projections thus threatening the habitability of Tuvalu.

Previous studies on coastal hazards in the tropical Pacific have often focussed on a single hazard such as waves generated by distant storms (Hoeke et al., 2013; Wandres et al., 2020), local tropical cyclones (Maragos et al., 1973), or storm surges (McInnes et al., 2014) and over small areas like a single beach or island (e.g., Storlazzi et al., 2018). Other studies have used empirical equations to estimate nearshore total water levels, and applied these regionally or globally (e.g., Vitousek et al., 2017; Vousdoukas et al., 2017, 2018, 2023), potentially missing some important physical processes (e.g., wave setup and IG waves). The methodology presented here can be efficiently applied across large areas in a mixed climate (regular and TC conditions) while maintaining a high spatial resolution and while resolving all necessary physical processes.

Recently, O'Grady et al. (2022) highlighted the need for special consideration when investigating extreme water levels in areas of mixed climates (i.e., in areas where the extreme water levels are driven by both cyclone and non-cyclone ocean conditions). The authors developed a formulation to account for two distinct extreme value distributions of TWL in a single mixed climate. However, to resolve non-linear wave transformation processes and translate TWL nearshore to coastal inundation in mixed-climate environments, a different approach is required. Here we present an alternative framework to estimate extreme water levels and coastal flooding in a mixed climate environment by treating the tropical cyclone and the regular climate independently. We performed Monte-Carlo simulations based on a non-parametric kernel density function combined with the simulation of thousands of years of extreme TC ocean conditions based on the STORM database (Bloemendaal et al., 2020). This method allowed us to explicitly map the multivariate drivers (wave conditions and offshore water levels) to the extreme nearshore TWL and flooding. We demonstrate that higher return interval floods are dominated by local tropical cyclones in the southern islands of Tuvalu (Figure 9a). More frequent events in the southern islands

are dominated by distant-source swell events ($T_p \geq \sim$13s). In the northern group, most occurring inundation (i.e., ARIs $\leq$ 100 years) is dominated by distant-source swells.

Changes in wave climate were not considered in this study as changes in waves are expected to only have minimal effects on inundation levels compared with changes in sea levels. However, as global warming continues, the frequency of tropical cyclones is anticipated to decrease while the intensity of tropical cyclones will increase (e.g., Knutson et al., 2010; Portner et al., 2019). Whether this will significantly alter the coastal flood hazard in Tuvalu remains subject to further study. Similarly, there is some discussion about the extent to which vertical accretion of coral reefs and reef islands will be able to keep up with sea level rise. Some evidence suggests that so far islands have not experienced any net erosion despite increased sea levels over recent decades (Beetham et al., 2017; Duvat, 2018; Kench et al., 2019; Webb & Kench, 2010). There is some doubt, however, that reef accretion rates will be able to keep up with accelerated rates of SLR, particularly if coral health degrades (Perry et al., 2018).

In general, the susceptibility of an atoll or reef island to coastal flooding largely depends on its bathymetry and topography. In extremely low-lying islands, a small increase in MSL leads to the inundation of most of the island's surface. Examples are Nukufetau, Nukulaelae, or Funafuti, where >89% of the atoll areas are projected to be flooded once every 5 years by 2100, irrespective of the climate change projection (Figure 12). On higher islands like Niulakita on the other hand, the flooded area increases approximately linearly with SLR. This becomes important when prioritizing adaptation measures for the different islands over the coming decades since higher islands are already naturally less vulnerable than lower lying atolls.

The methodology presented here can easily be upscaled to other islands in the Pacific region, where accurate baseline data are available. Unfortunately, many islands in the Pacific region have no established vertical reference datum and have never been properly surveyed. Freely available topographic data such as SRTM (Farr et al., 2007) have large uncertainties in low-lying islands making them inadequate for actionable inundation hazard assessments. The collection of high-resolution baseline data in low-lying areas should therefore be prioritized by donors and decision makers.

In line with other studies (Mycoo et al., 2022; Vitousek et al., 2017), our results indicate a significant increase in severity and frequency of extreme floods due to climate change, which will threaten the habitability of low-lying islands and atolls over the coming decades particularly, when considering the already limited access to freshwater resources or farmland (Duvat et al., 2021; Nakada et al., 2012; Storlazzi et al., 2018). In addition, a study by Taupo et al. (2018) found that poorer households in Tuvalu are more likely to reside in lower-lying areas closer to the coastline, exacerbating the risk to an already vulnerable group. The present study is therefore particularly important, allowing decision-makers to put policies and strategies into place to cope with the effect of sea level rise and coastal flooding on Tuvalu's population and key infrastructure. To that end, and to support Tuvalu's National Strategy for Sustainable Development (with regard to climate change and disaster resilience) the hazard information produced here, has already informed land reclamation and coastal adaptation initiatives that are currently underway in Tuvalu. Additionally, we created a graphical user interface that allows Tuvalu Government staff to navigate between different inundation scenarios and climate change projections and investigate the effect of various scenarios on the community and infrastructure. The system was deployed at the Tuvalu Government and is accessible through the intranet. A copy of the system is maintained by SPC (see Data Availability Statement).

Work is currently underway to translate the hazard data into risk information for population and infrastructure. This will enhance the actionability of the hazard products and in turn optimize their use within the Government of Tuvalu's decision-making process.

Data Availability Statement

The 44-year wave hindcast is hosted on the Pacific Community THREDDS server and can be accessed and downloaded through the following link: https://purl.org/spc/pdh/dataset/tuvalu-wave-hindcast_tds. Inundation hazard maps can be accessed via the Tuvalu Coastal Adaptation Project (TCAP) Dashboard through the following link: https://opm.gem.spc.int/tcap/inundation. The LiDAR digital elevation model (DEM) are not publicly available but can be made available upon request from the Government of Tuvalu. The data can be viewed through the following link: https://opm.gem.spc.int/tcap/DEM.

Acknowledgments
The work undertaken in this study was funded under the Tuvalu Coastal Adaptation Project (TCAP) implemented by the United Nations Development Programme (UNDP) through the Green Climate Fund (GCF). The authors would also like to thank the Pacific Community Centre for Ocean Sciences (PCCOS) and Jerome Aucan for the encouragement and for providing the time and resources to write this manuscript. The authors wish to acknowledge the use of New Zealand eScience Infrastructure (NeSI) high performance computing facilities, consulting support and/or training services as part of this research. New Zealand's national facilities are provided by NeSI and funded jointly by NeSI's collaborator institutions and through the Ministry of Business, Innovation & Employment's Research Infrastructure programme (https://www.nesi.org.nz). Finally, the authors thank Tuvalu's Lands and Survey Department, as well as SPC's technical workshop team for their contributions to the work.

References

Almar, R., Ranasinghe, R., Bergsma, E. W. J., Diaz, H., Melet, A., Papa, F., et al. (2021). A global analysis of extreme coastal water levels with implications for potential coastal overtopping. *Nature Communications*, *12*(1), 3775. https://doi.org/10.1038/s41467-021-24008-9

Andrew, N. L., Bright, P., de la Rua, L., Teoh, S. J., & Vickers, M. (2019). Coastal proximity of populations in 22 Pacific Island Countries and Territories. *PLoS One*, *14*(9), e0223249. https://doi.org/10.1371/journal.pone.0223249

Appendini, C. M., Torres-Freyermuth, A., Oropeza, F., Salles, P., López, J., & Mendoza, E. T. (2013). Wave modeling performance in the Gulf of Mexico and western Caribbean: Wind reanalyses assessment. *Applied Ocean Research*, *39*, 20–30. https://doi.org/10.1016/j.apor.2012.09.004

Arthur, W. C. (2021). A statistical-parametric model of tropical cyclones for hazard assessment. *Natural Hazards and Earth System Sciences*, *21*(3), 893–916. https://doi.org/10.5194/nhess-21-893-2021

Aung, T., Singh, A., & Prasad, U. (2009). Sea level threat in Tuvalu. *American Journal of Applied Sciences*, *6*(6), 1169–1174. https://doi.org/10.3844/ajassp.2009.1169.1174

Baldock, T. E. (2012). Dissipation of incident forced long waves in the surf zone—Implications for the concept of "bound" wave release at short wave breaking. *Coastal Engineering*, *60*(1), 276–285. https://doi.org/10.1016/j.coastaleng.2011.11.002

Barstow, S. F., & Haug, O. (1994). Wave climate of Tuvalu. *SOPAC Technical Report*, *203*, 1–26.

Becker, J. M., Merrifield, M. A., & Ford, M. (2014). Water level effects on breaking wave setup for Pacific Island fringing reefs. *Journal of Geophysical Research: Oceans*, *119*(2), 914–932. https://doi.org/10.1002/2013JC009373

Beetham, E., Kench, P. S., O'Callaghan, J., & Popinet, S. (2016). Wave transformation and shoreline water level on Funafuti Atoll, Tuvalu. *Journal of Geophysical Research: Oceans*, *121*(1), 311–326. https://doi.org/10.1002/2015JC011246

Beetham, E., Kench, P. S., & Popinet, S. (2017). Future reef growth can mitigate physical impacts of sea-level rise on atoll islands. *Earth's Future*, *5*(10), 1002–1014. https://doi.org/10.1002/2017EF000589

Beranger, B., Duong, T., Perkins-Kirkpatrick, S. E., & Sisson, S. A. (2016). Exploratory data analysis for moderate extreme values using non-parametric kernel methods.

Blacka, M. J., & Deiber, M. (2021). Nanumaga wave-driven inundation assessment, Tuvalu: Physical modelling report. https://www.wrl.unsw.edu.au/sites/wrl/files/uploads/Publications/WRL-TR-2021-19-Nanumaga-Wave-Driven-Inundation-Assessment-Tuvalu-Physical-Modelling-Report.pdf

Bloemendaal, N., Haigh, I. D., de Moel, H., Muis, S., Haarsma, R. J., & Aerts, J. C. J. H. (2020). Generation of a global synthetic tropical cyclone hazard dataset using STORM. *Scientific Data*, *7*(1), 1–12. https://doi.org/10.1038/s41597-020-0381-2

Boldi, M. O., & Davison, A. C. (2007). A mixture model for multivariate extremes. *Journal of the Royal Statistical Society—Series B: Statistical Methodology*, *69*(2), 217–229. https://doi.org/10.1111/j.1467-9868.2007.00585.x

Booij, N., Ris, R. C., & Holthuijsen, L. H. (1999). A third-generation wave model for coastal regions: 1. Model description and validation. *Journal of Geophysical Research*, *104*(C4), 7649–7666. https://doi.org/10.1029/98JC02622

Booji, N., Holthuijsen, L. H., & Ris, R. C. (1996). The SWAN wave model for shallow water. In *Proceedings of the 25th international conference on coastal engineering* (pp. 668–676).

Bosserelle, C., Lal, D., Movono, M., Begg, Z., Kumar, S., Reddy, S., et al. (2016). *Fatato (Tuvalu), oceanographic, topographic data collection*. Suva.

Bosserelle, C., Reddy, S., & Lal, D. (2015a). Funafuti wave buoy. In C. Bosserelle (Ed.), *WACOP wave climate reports. Secretariat of the Pacific community*.

Bosserelle, C., Reddy, S., & Lal, D. (2015b). WACOP wave climate reports.

Buckley, M., Lowe, R., & Hansen, J. (2014). Evaluation of nearshore wave models in steep reef environments. *Ocean Dynamics*, *64*(6), 847–862. https://doi.org/10.1007/s10236-014-0713-x

Camus, P., Losada, I. J., Izaguirre, C., Espejo, A., Menéndez, M., & Pérez, J. (2017). Statistical wave climate projections for coastal impact assessments. *Earth's Future*, *5*(9), 918–933. https://doi.org/10.1002/2017EF000609

Copernicus Climate Change Service (C3S). (2017). *ERA5: Fifth generation of ECMWF atmospheric reanalyses of the global climate*. Copernicus Climate Change Service Climate Data Store (CDS). https://doi.org/10.24381/cds.adbb2d47

Diamond, H. J., Lorrey, A. M., Knapp, K. R., & Levinson, D. H. (2012). Development of an enhanced tropical cyclone tracks database for the southwest Pacific from 1840 to 2010. *International Journal of Climatology*, *32*(14), 2240–2250. https://doi.org/10.1002/joc.2412

Durrant, T., Greenslade, D., Hemar, M., & Trenham, C. (2014). A global hindcast focussed on the central and South Pacific. CAWCR Technical Report No. 070 (Issue 070). Retrieved from http://www.cawcr.gov.au/technical-reports/CTR_070.pdf

Duvat, V. K. E. (2018). A global assessment of atoll island planform changes over the past decades. *WIREs Climate Change*, *10*(1). https://doi.org/10.1002/wcc.557

Duvat, V. K. E., Magnan, A. K., Perry, C. T., Spencer, T., Bell, J. D., Wabnitz, C. C. C., et al. (2021). Risks to future atoll habitability from climate-driven environmental changes. *WIREs Climate Change*, *12*(3). https://doi.org/10.1002/wcc.700

Egbert, G. D., & Erofeeva, S. Y. (2002). Efficient inverse modeling of barotropic ocean tides. *Journal of Atmospheric and Oceanic Technology*, *19*(2), 183–204. https://doi.org/10.1175/1520-0426(2002)019<0183:EIMOBO>2.0.CO;2

Farr, T. G., Rosen, P. A., Caro, E., Crippen, R., Duren, R., Hensley, S., et al. (2007). The shuttle radar topography mission. *Reviews of Geophysics*, *45*(2), RG2004. https://doi.org/10.1029/2005RG000183

Ford, M., Merrifield, M. A., & Becker, J. M. (2018). Inundation of a low-lying urban atoll island: Majuro, Marshall Islands. *Natural Hazards*, *91*(3), 1273–1297. https://doi.org/10.1007/s11069-018-3183-5

Franklin, G. L., & Torres-Freyermuth, A. (2022). On the runup parameterisation for reef-lined coasts. *Ocean Modelling*, *169*, 101929. https://doi.org/10.1016/j.ocemod.2021.101929

FUGRO. (2019). Report of survey airborne LiDAR acquisition across Tuvalu's nine atolls (Fugro Document No. TLCS 00.066.006).

Gouldby, B., Méndez, F. J., Guanche, Y., Rueda, A., & Mínguez, R. (2014). A methodology for deriving extreme nearshore sea conditions for structural design and flood risk analysis. *Coastal Engineering*, *88*, 15–26. https://doi.org/10.1016/j.coastaleng.2014.01.012

Government of Tuvalu. (2017). Tuvalu population & housing mini-census 2017 report.

Government of Tuvalu. (2020). Te Kete—Tuvalu national strategy for sustainable development 2021-2030.

Haigh, I. D., MacPherson, L. R., Mason, M. S., Wijeratne, E. M. S., Pattiaratchi, C. B., Crompton, R. P., & George, S. (2014). Estimating present day extreme water level exceedance probabilities around the coastline of Australia: Tropical cyclone-induced storm surges. *Climate Dynamics*, *42*(1–2), 139–157. https://doi.org/10.1007/s00382-012-1653-0

Hoeke, R. K., Damlamian, H., Aucan, J., & Wandres, M. (2021). Severe flooding in the atoll nations of Tuvalu and Kiribati triggered by a distant Tropical Cyclone Pam. *Frontiers in Marine Science*, *7*, 1–12. https://doi.org/10.3389/fmars.2020.539646

Hoeke, R. K., McInnes, K. L., Kruger, J. C., McNaught, R. J., Hunter, J. R., & Smithers, S. G. (2013). Widespread inundation of Pacific islands triggered by distant-source wind-waves. *Global and Planetary Change*, *108*, 128–138. https://doi.org/10.1016/j.gloplacha.2013.06.006

Holland, G. J. (1980). An analytic model of the wind and pressure profiles in hurricanes. *Monthly Weather Review*, *108*(8), 1212–1218. https://doi.org/10.1175/1520-0493(1980)108<1212:AAMOTW>2.0.CO;2

Izaguirre, C., Mendez, F. J., Menendez, M., Luceño, A., & Losada, I. J. (2010). Extreme wave climate variability in southern Europe using satellite data. *Journal of Geophysical Research*, *115*(C4), C04009. https://doi.org/10.1029/2009JC005802

Joyce, B. R., Gonzalez-Lopez, J., Van der Westhuysen, A. J., Yang, D., Pringle, W. J., Westerink, J. J., & Cox, A. T. (2019). U.S. IOOS coastal and ocean modeling testbed: Hurricane-induced winds, waves, and surge for deep ocean, reef-fringed islands in the Caribbean. *Journal of Geophysical Research: Oceans*, *124*(4), 2876–2907. https://doi.org/10.1029/2018JC014687

Kench, P. S., Ford, M. R., & Owen, S. D. (2019). Patterns of island change and persistence offer alternate adaptation pathways for atoll nations. *Nature Communications*, *9*(1), 605. https://doi.org/10.1038/s41467-018-02954-1

Kepert, J. (2001). The dynamics of boundary layer jets within the tropical cyclone core. Part I: Linear theory. *Journal of the Atmospheric Sciences*, *58*(17), 2469–2484. https://doi.org/10.1175/1520-0469(2001)058<2469:TDOBLJ>2.0.CO;2

Klaver, S., Nederhoff, C. M., Giardino, A., Tissier, M. F. S., Dongeren, A. R., & Spek, A. J. F. (2019). Impact of coral reef mining pits on nearshore hydrodynamics and wave runup during extreme wave events. *Journal of Geophysical Research: Oceans*, *124*(4), 2824–2841. https://doi.org/10.1029/2018JC014165

Knaff, J. A., Slocum, C. J., Musgrave, K. D., Sampson, C. R., & Strahl, B. R. (2016). Using routinely available information to estimate tropical cyclone wind structure. *Monthly Weather Review*, *144*(4), 1233–1247. https://doi.org/10.1175/MWR-D-15-0267.1

Knutson, T. R., McBride, J. L., Chan, J., Emanuel, K., Holland, G., Landsea, C., et al. (2010). Tropical cyclones and climate change. *Nature geoscience*, *3*(3), 157–163. https://doi.org/10.1038/ngeo779

Koons, H. C. (2001). Statistical analysis of extreme values in space science. *Journal of Geophysical Research*, *106*(A6), 10915–10921. https://doi.org/10.1029/2000ja000234

Krüger, J. (2008). High-resolution bathymetric survey of Tuvalu. EU EDF 8—SOPAC project report 50. http://www.sopac.org

Lashley, C. H., Roelvink, D., van Dongeren, A., Buckley, M. L., & Lowe, R. J. (2018). Nonhydrostatic and surfbeat model predictions of extreme wave run-up in fringing reef environments. *Coastal Engineering*, *137*, 11–27. https://doi.org/10.1016/j.coastaleng.2018.03.007

Li, F., Bicknell, C., Lowry, R., & Li, Y. (2012). A comparison of extreme wave analysis methods with 1994-2010 offshore Perth dataset. *Coastal Engineering*, *69*, 1–11. https://doi.org/10.1016/j.coastaleng.2012.05.006

Liu, Y., Li, S., Liao, Z., Liu, Q., Zou, Q., & Liu, W. (2023). Explicit wave-runup formula for beaches fronted by coral reefs using tree-based models. *Coastal Engineering*, *104308*, 104308. https://doi.org/10.1016/j.coastaleng.2023.104308

MacDonald, A., Scarrott, C. J., Lee, D., Darlow, B., Reale, M., & Russell, G. (2011). A flexible extreme value mixture model. *Computational Statistics & Data Analysis*, *55*(6), 2137–2157. https://doi.org/10.1016/j.csda.2011.01.005

Maragos, J. E., Baines, G. B. K., & Beveridge, P. J. (1973). Tropical cyclone Bebe creates a new land formation on Funafuti Atoll. *Science*, *181*(4105), 1161–1164. https://doi.org/10.1126/science.181.4105.1161

Marra, J. J., Gooley, G., Johnson, M.-V., Keener, V., Kruk, M. K., McGree, S., et al. (2022). Pacific Islands climate change monitor: 2021.

McInnes, K. L., Walsh, K. J. E., Hoeke, R. K., O'Grady, J. G., Colberg, F., & Hubbert, G. D. (2014). Quantifying storm tide risk in Fiji due to climate variability and change. *Global and Planetary Change*, *116*, 115–129. https://doi.org/10.1016/j.gloplacha.2014.02.004

Mclean, R. F., & Hosking, P. L. (1991). Geomorphology of reef islands and atoll motu in Tuvalu. *The South Pacific Journal of Natural Science*, *11*, 167–189.

Méndez, F. J., Menéndez, M., Luceño, A., & Losada, I. J. (2007). Analyzing monthly extreme sea levels with a time-dependent GEV model. *Journal of Atmospheric and Oceanic Technology*, *24*(5), 894–911. https://doi.org/10.1175/JTECH2009.1

Merrifield, M. A., Becker, J. M., Ford, M., & Yao, Y. (2014). Observations and estimates of wave-driven water level extremes at the Marshall Islands. *Geophysical Research Letters*, *41*(20), 7245–7253. https://doi.org/10.1002/2014GL061005

Merrifield, M. A., Johnson, M., Guza, R. T., Fiedler, J. W., Young, A. P., Henderson, C. S., et al. (2021). An early warning system for wave-driven coastal flooding at Imperial Beach, CA. *Natural Hazards*, *108*(3), 2591–2612. https://doi.org/10.1007/s11069-021-04790-x

Moftakhari, H. R., AghaKouchak, A., Sanders, B. F., Allaire, M., & Matthew, R. A. (2018). What is nuisance flooding? Defining and monitoring an emerging challenge. *Water Resources Research*, *54*(7), 4218–4227. https://doi.org/10.1029/2018WR022828

Munk, W. H., & Sargent, M. C. (1948). Adjustment of Bikini Atoll to ocean waves. *Eos, Transactions American Geophysical Union*, *29*(6), 855–860. https://doi.org/10.1029/TR029i006p00855

Murakami, H. (2014). Tropical cyclones in reanalysis data sets. *Geophysical Research Letters*, *41*(6), 2133–2141. https://doi.org/10.1002/2014GL059519.Received

Mycoo, M., Wairiu, M., Campbell, D., Duvat, V., Golbuu, Y., Maharaj, S., et al. (2022). Small islands. In H.-O. Pörtner, D. C. Roberts, M. Tignor, E. S. Poloczanska, K. Mintenbeck, A. Alegría, et al. (Eds.), *Climate change 2022: Impacts, adaptation and vulnerability. Contribution of working group II to the sixth assessment report of the intergovernmental panel on climate change* (pp. 2043–2121). Cambridge University Press. https://doi.org/10.1017/9781009325844.017

Nakada, S., Umezawa, Y., Taniguchi, M., & Yamano, H. (2012). Groundwater dynamics of Fongafale Islet, Funafuti Atoll, Tuvalu. *Ground Water*, *50*(4), 639–644. https://doi.org/10.1111/j.1745-6584.2011.00874.x

O'Grady, J. G., McInnes, K. L., Hemer, M. A., Hoeke, R. K., Stephenson, A. G., & Colberg, F. (2019). Extreme water levels for Australian beaches using empirical equations for shoreline wave setup. *Journal of Geophysical Research: Oceans*, *124*(8), 5468–5484. https://doi.org/10.1029/2018JC014871

O'Grady, J. G., Stephenson, A. G., & McInnes, K. L. (2022). Gauging mixed climate extreme value distributions in tropical cyclone regions. *Scientific Reports*, *12*(1), 4626. https://doi.org/10.1038/s41598-022-08382-y

Ohde, S., Greaves, M., Masuzawa, T., Buckley, H. A., Van Woesik, R., Wilson, P. A., et al. (2002). The chronology of Funafuti Atoll: Revisiting an old friend. *Proceedings of the Royal Society of London. Series A: Mathematical, Physical and Engineering Sciences*, *458*(2025), 2289–2306. https://doi.org/10.1098/rspa.2002.0978

Oliveira, J. N. C., Oliveira, F. S. B. F., Neves, M. G., Clavero, M., & Trigo-Teixeira, A. A. (2020). Modeling wave overtopping on a seawall with XBeach, IH2VOF, and mase formulas. *Water*, *12*(9), 2526. https://doi.org/10.3390/w12092526

Patel, S. S. (2006). A sinking feeling. *Nature*, *440*(7085), 734–736. https://doi.org/10.1038/440734a

Pearson, S. G., Storlazzi, C. D., van Dongeren, A. R., Tissier, M. F. S., & Reniers, A. J. H. M. (2017). A Bayesian-based system to assess wave-driven flooding hazards on coral reef-lined coasts. *Journal of Geophysical Research: Oceans*, *122*(12), 10099–10117. https://doi.org/10.1002/2017JC013204

Perry, C. T., Alvarez-Filip, L., Graham, N. A. J., Mumby, P. J., Wilson, S. K., Kench, P. S., et al. (2018). Loss of coral reef growth capacity to track future increases in sea level. *Nature*, *558*(7710), 396–400. https://doi.org/10.1038/s41586-018-0194-z

Pomeroy, A., Lowe, R., Symonds, G., van Dongeren, A., & Moore, C. (2012). The dynamics of infragravity wave transformation over a fringing reef. *Journal of Geophysical Research*, *117*(11), 1–17. https://doi.org/10.1029/2012JC008310

Portner, H. O., Roberts, D. C., Masson-Delmotte, V., Zhai, P., Tignor, M., Poloczanska, E., et al. (2019). IPCC the ocean and cryosphere in a changing climate summary for policmakers. *IPCC Special Report on the Ocean and Cryosphere in a Changing Climate, September, SPM-1-SPM-42*. https://report.ipcc.ch/srocc/pdf/SROCC_SPM_Approved.pdf

Powell, M., Soukup, G., Cocke, S., Gulati, S., Morisseau-Leroy, N., Hamid, S., et al. (2005). State of Florida hurricane loss projection model: Atmospheric science component. *Journal of Wind Engineering and Industrial Aerodynamics*, *93*(8), 651–674. https://doi.org/10.1016/j.jweia.2005.05.008

PRIF. (2021). Guidance for managing sea level rise infrastructure risk in Pacific Island countries. Retrieved from www.theprif.org

Quataert, E., Storlazzi, C., van Rooijen, A., Cheriton, O., & van Dongeren, A. (2015). The influence of coral reefs and climate change on wave-driven flooding of tropical coastlines. *Geophysical Research Letters*, *42*(15), 6407–6415. https://doi.org/10.1002/2015GL064861

Rached, I., & Larsson, E. (2019). Tail distribution and extreme quantile estimation using non-parametric approaches. In J. Kołodziej, & H. González-Vélez (Eds.), *High-performance modelling and simulation for big data applications*, *Lecture notes in computer science* (Vol. 11400, pp. 69–87). Springer International Publishing. https://doi.org/10.1007/978-3-030-16272-6_3

Ritman, M., Hague, B., Katea, T., Vaaia, T., Ngari, A., Smith, G., et al. (2022). Past and future coastal flooding in Pacific small-island nations: Insights from the Pacific Sea Level and Geodetic Monitoring (PSLGM) project tide gauges. *Journal of Southern Hemisphere Earth Systems Science*, *72*(3), 202–217. https://doi.org/10.1071/ES22023

Roberts, K. J., Pringle, W. J., & Westerink, J. J. (2019). OceanMesh2D 1.0: MATLAB-based software for two-dimensional unstructured mesh generation in coastal ocean modeling. *Geoscientific Model Development*, *12*(5), 1847–1868. https://doi.org/10.5194/gmd-12-1847-2019

Roelvink, D., McCall, R., Mehvar, S., Nederhoff, K., & Dastgheib, A. (2018). Improving predictions of swash dynamics in XBeach: The role of groupiness and incident-band runup. *Coastal Engineering*, *134*, 103–123. https://doi.org/10.1016/j.coastaleng.2017.07.004

Roelvink, D., Reniers, A., van Dongeren, A., van Thiel de Vries, J., McCall, R., & Lescinski, J. (2009). Modelling storm impacts on beaches, dunes and barrier islands. *Coastal Engineering*, *56*(11–12), 1133–1152. https://doi.org/10.1016/j.coastaleng.2009.08.006

Rueda, A., Cagigal, L., Pearson, S., Antolínez, J. A. A., Storlazzi, C., van Dongeren, A., et al. (2019). HyCReWW: A hybrid coral reef wave and water level metamodel. *Computers & Geosciences*, *127*, 85–90. https://doi.org/10.1016/j.cageo.2019.03.004

Rueda, A., Camus, P., Tomás, A., Vitousek, S., & Méndez, F. J. (2016). A multivariate extreme wave and storm surge climate emulator based on weather patterns. *Ocean Modelling*, *104*, 242–251. https://doi.org/10.1016/j.ocemod.2016.06.008

Rueda, A., Gouldby, B., Méndez, F. J., Tomás, A., Losada, I. J., Lara, J. L., & Díaz-Simal, P. (2016). The use of wave propagation and reduced complexity inundation models and metamodels for coastal flood risk assessment. *Journal of Flood Risk Management*, *9*(4), 390–401. https://doi.org/10.1111/jfr3.12204

Shope, J. B., Storlazzi, C. D., Erikson, L. H., & Hegermiller, C. A. (2016). Changes to extreme wave climates of islands within the Western Tropical Pacific throughout the 21st century under RCP 4.5 and RCP 8.5, with implications for island vulnerability and sustainability. *Global and Planetary Change*, *141*, 25–38. https://doi.org/10.1016/j.gloplacha.2016.03.009

Smit, P., Stelling, G., Roelvink, J., de Vries, J. V. T., McCall, R., Van Dongeren, A., et al. (2010). XBeach: Non-hydrostatic model.

Stockdon, H. F., Holman, R. A., Howd, P. A., & Sallenger, A. H. (2006). Empirical parameterization of setup, swash, and runup. *Coastal Engineering*, *53*(7), 573–588. https://doi.org/10.1016/j.coastaleng.2005.12.005

Stockdon, H. F., Long, J. W., Palmsten, M. L., van der Westhuysen, A., Doran, K. S., & Snell, R. J. (2023). Operational forecasts of wave-driven water levels and coastal hazards for US Gulf and Atlantic coasts. *Communications Earth & Environment*, *4*(1), 169. https://doi.org/10.1038/s43247-023-00817-2

Storlazzi, C., Reguero, B. G., Cole, A. D., Lowe, E., Shope, J. B., Gibbs, A. E., et al. (2019). Rigorously valuing the role of U.S. Coral reefs in coastal hazard risk reduction. *U.S.Geological Survey Open-File Report 2021–1054*, 42. https://doi.org/10.3133/ofr20191027

Storlazzi, C. D., Gingerich, S. B., van Dongeren, A., Cheriton, O. M., Swarzenski, P. W., Quataert, E., et al. (2018). Most atolls will be uninhabitable by the mid-21st century because of sea-level rise exacerbating wave-driven flooding. *Science Advances*, *4*(4), 1–10. https://doi.org/10.1126/sciadv.aap9741

Tait, R. J. (1972). Wave set-up on coral reefs. *Journal of Geophysical Research*, *77*(12), 2207–2211. https://doi.org/10.1029/jc077i012p02207

Taupo, T., Cuffe, H., & Noy, I. (2018). Household vulnerability on the frontline of climate change: The Pacific atoll nation of Tuvalu. *Environmental Economics and Policy Studies*, *20*(4), 705–739. https://doi.org/10.1007/s10018-018-0212-2

Tuck, M. E., Ford, M. R., Masselink, G., & Kench, P. S. (2019). Geomorphology physical modelling of reef island topographic response to rising sea levels. *Geomorphology*, *345*, 106833. https://doi.org/10.1016/j.geomorph.2019.106833

Tu'uholoaki, M., Espejo, A., Wandres, M., Singh, A., Damlamian, H., & Begg, Z. (2023). Quantifying mechanisms responsible for extreme coastal water levels and flooding during severe tropical cyclone Harold in Tonga, southwest Pacific. *Journal of Marine Science and Engineering*, *11*(6), 1217. https://doi.org/10.3390/jmse11061217

Tuvalu Meteorological Service. (2018). The Tuvalu meteorological services' report on large waves (southerly swells) 25th–30th May 2018. (Issue May).

van Dongeren, A., Lowe, R., Pomeroy, A., Trang, D. M., Roelvink, D., Symonds, G., & Ranasinghe, R. (2013). Numerical modeling of low-frequency wave dynamics over a fringing coral reef. *Coastal Engineering*, *73*, 178–190. https://doi.org/10.1016/j.coastaleng.2012.11.004

Vetter, O., Becker, J. M., Merrifield, M. A., Pequignet, A. C., Aucan, J., Boc, S. J., & Pollock, C. E. (2010). Wave setup over a Pacific Island fringing reef. *Journal of Geophysical Research*, *115*(12), C12066. https://doi.org/10.1029/2010JC006455

Vitousek, S., Barnard, P. L., Fletcher, C. H., Frazer, N., Erikson, L., & Storlazzi, C. D. (2017). Doubling of coastal flooding frequency within decades due to sea-level rise. *Scientific Reports*, *7*(1), 1–9. https://doi.org/10.1038/s41598-017-01362-7

Vousdoukas, M. I., Athanasiou, P., Giardino, A., Mentaschi, L., Stocchino, A., Kopp, R. E., et al. (2023). Small Island Developing States under threat by rising seas even in a 1.5°C warming world. *Nature Sustainability*, *6*(12), 1552–1564. https://doi.org/10.1038/s41893-023-01230-5

Vousdoukas, M. I., Mentaschi, L., Voukouvalas, E., Verlaan, M., & Feyen, L. (2017). Extreme sea levels on the rise along Europe's coasts. *Earth's Future*, *5*(3), 304–323. https://doi.org/10.1002/2016EF000505

Vousdoukas, M. I., Mentaschi, L., Voukouvalas, E., Verlaan, M., Jevrejeva, S., Jackson, L. P., & Feyen, L. (2018). Global probabilistic projections of extreme sea levels show intensification of coastal flood hazard. *Nature Communications*, *9*(1), 2360. https://doi.org/10.1038/s41467-018-04692-w

Wandres, M., Aucan, J., Espejo, A., Jackson, N., de Ramon N'Yeurt, A., & Damlamian, H. (2020). Distant-source swells cause coastal inundation on Fiji's coral coast. *Frontiers in Marine Science*, *7*, 1–10. https://doi.org/10.3389/fmars.2020.00546

Wandres, M., Espejo, A., & Damlamian, H. (2023). Wave climate variability and trends in Tuvalu based on a 44-year high-resolution wave hindcast. *Journal of Geophysical Research: Oceans*, *128*(4), e2022JC019523. https://doi.org/10.1029/2022JC019523

Webb, A. (2007). Tuvalu technical report, assessment of salinity of groundwater in swamp taro (cyrtosperma chamissonis) "pulaka" pits in Tuvalu. https://www.researchgate.net/publication/328175697

Webb, A. P., & Kench, P. S. (2010). The dynamic response of reef islands to sea-level rise: Evidence from multi-decadal analysis of island change in the Central Pacific. *Global and Planetary Change*, *72*(3), 234–246. https://doi.org/10.1016/j.gloplacha.2010.05.003

Wu, W., Westra, S., & Leonard, M. (2021). Estimating the probability of compound floods in estuarine regions. *Hydrology and Earth System Sciences*, *25*(5), 2821–2841. https://doi.org/10.5194/hess-25-2821-2021

Yamano, H., Kayanne, H., Yamaguchi, T., Kuwahara, Y., Yokoki, H., Shimazaki, H., & Chikamori, M. (2007). Atoll island vulnerability to flooding and inundation revealed by historical reconstruction: Fongafale Islet, Funafuti Atoll, Tuvalu. *Global and Planetary Change*, *57*(3–4), 407–416. https://doi.org/10.1016/j.gloplacha.2007.02.007

Zambom, A. Z., & Dias, R. (2012). A review of Kernel density estimation with applications to econometrics. *International Econometric Review (IER)*, 20–42.

Zijlema, M., Stelling, G., & Smit, P. (2011). SWASH: An operational public domain code for simulating wave fields and rapidly varied flows in coastal waters. *Coastal Engineering*, *58*(10), 992–1012. https://doi.org/10.1016/j.coastaleng.2011.05.015

Zijlema, M., van Vledder, G. P., & Holthuijsen, L. H. (2012). Bottom friction and wind drag for wave models. *Coastal Engineering*, *65*, 19–26. https://doi.org/10.1016/j.coastaleng.2012.03.002

Zuo, H., Balmaseda, M. A., Tietsche, S., Mogensen, K., & Mayer, M. (2019). The ECMWF operational ensemble reanalysis-analysis system for ocean and sea ice: A description of the system and assessment. *Ocean Science*, *15*(3), 779–808. https://doi.org/10.5194/os-15-779-2019